JOURNAL OF GEOPHYSICAL RESEARCH, VOL. 115, B06408, doi:10.1029/2009JB006645, 2010

Fore-arc deformation and underplating at the northern Hikurangi margin, New Zealand

M. Scherwath,[1,2] H. Kopp,[1] E. R. Flueh,[1] S. A. Henrys,[3] R. Sutherland,[3] V. M. Stagpoole,[3] D. H. N. Barker,[3] M. E. Reyners,[3] D. G. Bassett,[4] L. Planert,[1] and A. Dannowski[1]

Received 25 May 2009; revised 9 December 2009; accepted 27 January 2010; published 25 June 2010.

[1] Geophysical investigations of the northern Hikurangi subduction zone northeast of New Zealand, image fore-arc and surrounding upper lithospheric structures. A seismic velocity (Vp) field is determined from seismic wide-angle data, and our structural interpretation is supported by multichannel seismic reflection stratigraphy and gravity and magnetic modeling. We found that the subducting Hikurangi Plateau carries about 2 km of sediments above a 2 km mixed layer of volcaniclastics, limestone, and chert. The upper plateau crust is characterized by Vp = 4.9–6.7 km/s overlying the lower crust with Vp > 7.1 km/s. Gravity modeling yields a plateau thickness around 10 km. The reactivated Raukumara fore-arc basin is >10 km deep, deposited on 5–10 km thick Australian crust. The fore-arc mantle of Vp > 8 km/s appears unaffected by subduction hydration processes. The East Cape Ridge fore-arc high is underlain by a 3.5 km deep strongly magnetic (3.3 A/m) high-velocity zone, interpreted as part of the onshore Matakaoa volcanic allochthon and/or uplifted Raukumara Basin basement of probable oceanic crustal origin. Beneath the trench slope, we interpret low-seismic-velocity, high-attenuation, low-density fore-arc material as accreted and recycled, suggesting that underplating and uplift destabilizes East Cape Ridge, triggering two-sided mass wasting. Mass balance calculations indicate that the proposed accreted and recycled material represents 25–100% of all incoming sediment, and any remainder could be accounted for through erosion of older accreted material into surrounding basins. We suggest that continental mass flux into the mantle at subduction zones may be significantly overestimated because crustal underplating beneath fore-arc highs have not properly been accounted for.

Citation: Scherwath, M., et al. (2010), Fore-arc deformation and underplating at the northern Hikurangi margin, New Zealand, *J. Geophys. Res.*, *115*, B06408, doi:10.1029/2009JB006645.

1. Introduction

[2] Understanding and quantifying how mass transfer processes vary in space and time at subduction zones is essential to address questions surrounding the long-term growth of continents [e.g., *Rudnick and Fountain*, 1995]. The balance of sediment accretion, subduction erosion, and addition of mantle-derived material in the magmatic arc determines if a convergent margin is a site of net crustal growth or destruction. The structure of accretionary wedges and erosional margins is now well imaged in classic reflection seismic lines [e.g., *Davey et al.*, 1986; *Ye et al.*, 1997; *Park et al.*, 2002; *Kopp and Kukowski*, 2003; *von Huene et al.*, 2004], and many analogue and numerical simulations dedicated to convergent margin processes have focused on both the growth and erosion of convergent margins [e.g., *Davis et al.*, 1983; *Gutscher et al.*, 1998; *Upton et al.*, 2003; *Litchfield et al.*, 2007]. Based on such data and models, the global fluxes of subducted sediment and continental material have been estimated [*von Huene and Scholl*, 1991; *Clift and Vannucchi*, 2004], but large uncertainties remain. In this paper, we present new geophysical data from the northern Hikurangi margin, New Zealand, and challenge some of the assumptions that underpin estimates of global crustal fluxes in subduction zones.

[3] The processes of fore-arc crustal accretion or erosion are causally related to the behavior of the subduction thrust and faults within both the footwall and hanging wall, so our results have significance for understanding seismic hazard. Subduction zones typically show significant along-strike variability and it is clear that deep fore-arc basins point to significant regional tectonic controls on processes occurring at the plate interface, with implications for the nucleation and propagation of large-magnitude subduction earthquakes

[1]Leibniz Institute of Marine Sciences, IFM-GEOMAR, Kiel, Germany.
[2]Now at School of Earth and Ocean Sciences, University of Victoria, Victoria, British Columbia, Canada.
[3]GNS Science, Lower Hutt, New Zealand.
[4]School of Geography, Environment and Earth Sciences, Victoria University of Wellington, Wellington, New Zealand.

0148-0227/10/2009JB006645

[*Song and Simons*, 2003; *Wells et al.*, 2003]. For most subduction zones, the details of the spatial and temporal relationships between subduction accretion, erosion processes, fore-arc basin subsidence, and regional uplift patterns remain largely unresolved. However, it has been suggested that there is a correlation between the locations of large earthquakes, fore-arc basins, and gravity lows; and permanent interseismic subsidence is inferred to have been caused by plate coupling and long-term subduction erosion in those regions [*Song and Simons*, 2003; *Wells et al.*, 2003].

[4] The northern Hikurangi margin and Raukumara Peninsula of New Zealand (Figure 1) provide an ideal setting to examine these along-strike processes, because a broad range of complementary data types are available and marked differences in morphology and geological structure along and across the margin point to significant changes in subduction mechanics. The Hikurangi Plateau, a Cretaceous Large Igneous Province of the Pacific Plate [*Davy and Wood*, 1994; *Mortimer and Parkinson*, 1996], is subducting westward at approximately 60 mm/yr relative to the fore arc, causing active uplift of Raukumara Peninsula [*Litchfield et al.*, 2007; *Wilson et al.*, 2007], but farther to the east the outer trench slope is steep and subject to basal tectonic erosion [*Collot et al.* 1996; *Davey et al.*, 1997; *Barker et al.*, 2009]. Along strike towards the north, Raukumara Peninsula is replaced by a deep (>12 km) sedimentary basin coincident with a prominent –140 mgal gravity low, and is bounded to the east by a protuberant outer fore-arc high and a steep frontal margin wedge.

[5] Recently, *Sutherland et al.* [2009] presented an overview of new seismic reflection (RAU07) and refraction data acquired in 2007. These data provide a clear image of Raukumara Basin, the underlying Australian crust and subducting slab. The RAU07 data allow the stratigraphy of Raukumara Basin and some of the large-scale structure to be mapped out. *Sutherland et al.* [2009] divided the reflection strata defining Raukumara Basin into three sedimentary megasequences which they correlated with the onshore geology. The oldest sequence is interpreted as late Cretaceous and Paleogene passive margin sediments overlain by a sequence of Early Miocene allochthonous material and Neogene marine sedimentary rocks. In addition, they present a new kinematic model of the fore arc that involved frontal subduction erosion and basal accretion of the eroded material into the lower crust of the hanging wall.

[6] In this paper, we present a detailed analysis of seismic wide-angle reflection and refraction data collected along a dip profile through Raukumara Basin and across the subduction zone to the footwall. Our seismic velocity image is combined with the stratigraphy from multichannel seismic reflection profiles and ship-borne gravity and magnetic data to yield structural constraints that allow us to place constraints on the structure of Raukumara Basin and thickness of basin fill. The new velocity image also more precisely helps identify and quantify subduction processes within the upper 20 km, which in this case of relatively thin hanging wall crust includes the Moho, crust, and the accreted fore-arc material.

2. Tectonic Setting

[7] The region immediately northeast of the North Island of New Zealand (Figure 1), marks a transition from the Tonga-Kermadec to the Hikurangi subduction zone. The region includes a north-to-south transition on the downgoing Pacific plate from typical oceanic crust to anomalously thick oceanic crust of the Hikurangi Plateau (Rapuhia scarp, Figure 1) [*Davy and Collot*, 2000], and on the overriding plate from thin crust of possibly oceanic type to continental crust of 30–40 km thickness [*Reyners et al.*, 1999, 2006; *Sutherland et al.*, 2009]. The Cretaceous Hikurangi Plateau [*Mortimer and Parkinson*, 1996] has a crustal thickness of about 10–15 km to the east of Raukumara Peninsula [*Davy and Wood*, 1994]. The anomalous nature of this subducting plateau is implicated in models for uplift of the East Coast of the North Island and exposure of the fore arc [*Litchfield et al.*, 2007]. Geodetic measurements and active faulting indicate that the eastern part of the peninsula is currently extending normal to the plate margin [*Thornley*, 1996] and has experienced up to 6 km of extension since the Pliocene [*Nicol et al.*, 2007].

[8] In the region of the northern Hikurangi margin, the Pacific and Australian plates are converging obliquely at about 45 mm/yr [*DeMets et al.*, 1994] (Figure 1), but back-arc spreading in the Havre Trough and central North Island result in almost orthogonal convergence across the subduction thrust at approximately 60 mm/yr [*Wallace et al.*, 2004]. The general shape of the subducted plate has been revealed by compilations of seismicity from the IRIS Data Management Center, the New Zealand national seismograph network, and through a series of temporary deployments of dense networks of portable seismographs [*Reyners et al.*, 1999, 2006]. The continental crust is ~20 km thick beneath the northern Raukumara Peninsula and thickens to greater than 35 km to the south, as inferred from crustal seismic P wave velocity (Vp) estimates of 5.5–6.5 km/s [*Reyners et al.*, 1999, 2006; *Sutherland et al.*, 2009]. Earthquake hypocenters cluster within the upper part of the subducting plate at 15 km depth, and in the crust between the east coast of Raukumara Peninsula and the subduction front. The uppermost approximately 10 km of the mantle of the subducted slab consistently has Vp > 8.5 km/s, and reduces to more normal mantle velocities of approximately Vp = 8.2 km/s beneath [*Reyners et al.*, 1999]. Earthquake focal mechanisms indicate downdip tensional strain within

Figure 1. Regional base map, southwest Pacific, northeast of North Island, New Zealand (see small, gray scale inset for a global overview). The data profile corresponds to the seismic wide-angle data transect MANGO-1, seismic reflection line RAU07-05 and available ship-borne gravity and magnetic profiles. Yellow triangles mark locations of mapped volcanoes, and orange circles represent earthquakes larger magnitude 4.0 since 1990, scaled according to size. Plate motion of the Pacific relative to the Australian plate [after *DeMets et al.*, 1994]. Onshore Raukumara Peninsula simplified geology [after *Mazengarb and Speden*, 2000] and uplift [after *Litchfield et al.*, 2007], and offshore locations of the ocean bottom seismic receivers with those stations annotated whose data are shown in Figure 2.

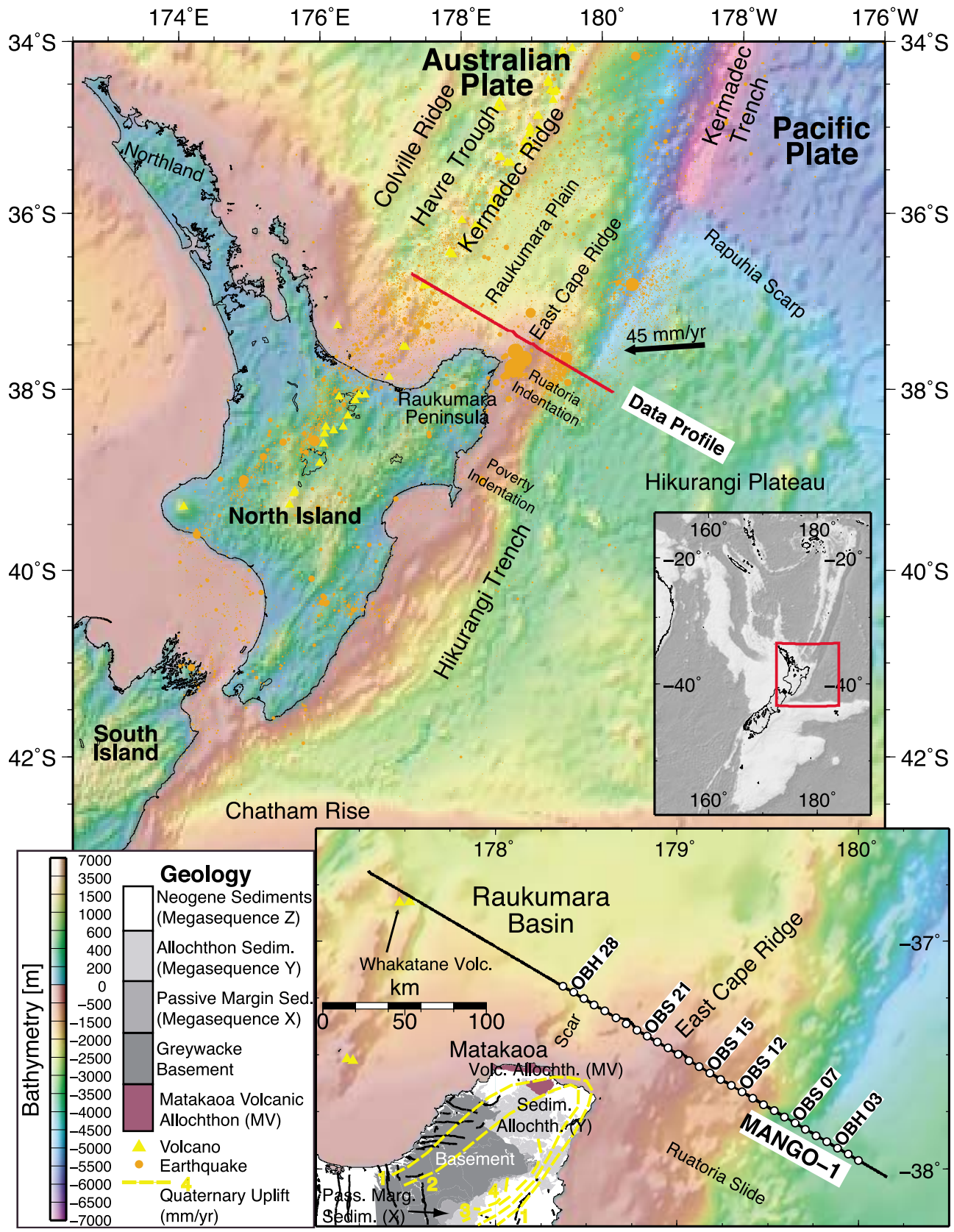
174°E
176°E
178°E
180°
178°W
176°W
34°S
36°S
38°S
40°S
42°S
Australian Plate
Pacific Plate
Colville Ridge
Havre Trough
Kermadec Ridge
Kermadec Trench
Raukumara Plain
East Cape Ridge
Rapuhia Scarp
45 mm/yr
Ruatoria Indentation
Data Profile
Raukumara Peninsula
Poverty Indentation
Hikurangi Plateau
Hikurangi Trench
Northland
North Island
South Island
Chatham Rise
160°
180°
−20°
−40°
Bathymetry [m]
7000
3500
1500
1000
600
400
200
0
−500
−1500
−2000
−2500
−3000
−3500
−4000
−4500
−5000
−5500
−6000
−6500
−7000
Geology
Neogene Sediments (Megasequence Z)
Allochthon Sedim. (Megasequence Y)
Passive Margin Sed. (Megasequence X)
Greywacke Basement
Matakaoa Volcanic Allochthon (MV)
Volcano
Earthquake
Quaternary Uplift (mm/yr)
178°
179°
180°
Raukumara Basin
Whakatane Volc.
km
0
50
100
OBH 28
OBS 21
East Cape Ridge
OBS 15
OBS 12
OBS 07
OBH 03
MANGO−1
−37°
−38°
Scar
Matakaoa Volc. Allochth. (MV)
Sedim. Allochth. (Y)
Basement
Pass. Marg. Sedim. (X)
Ruatoria Slide

Figure 1

the subducting plate, and NNW–SSE extensional strain within the shallow part of the upper plate [*Reyners and McGinty*, 1999], consistent with geological and geodetic observations [*Árnadóttir et al.*, 1999]. The seismogenic zone has well-constrained changes in plate coupling, where the coupling zone is shallower at the northern Hikurangi margin but deeper to the south where the risk of large megathrust earthquakes is also higher, though the interplay of the coupling parameters such as plate structure and fluid pressure is rather complex [*Wallace et al.*, 2009].

[9] Onshore, Raukumara Peninsula can be divided into distinct geological units [*Mazengarb and Harris*, 1994; *Field et al.*, 1997; *Mazengarb and Speden*, 2000] (Figure 1) that can also be recognized offshore as seismic reflection megasequences [*Sutherland et al.*, 2009]: (1) a western unit of Early Cretaceous greywacke basement in the Raukumara Range; (2) Late Cretaceous and Paleogene marine passive margin sediments (megasequence X); (3) the East Coast allochthon (megasequence Y), a belt of Late Cretaceous and Early Tertiary rocks that were thrust towards the southwest over units 1 and 2 during the earliest Miocene, and the East Coast allochthon, together with the enigmatic Matakaoa volcanic rocks, are considered concomitant with the emplacement of the Northland ophiolite terrane of northern New Zealand [*Whattam et al.*, 2004] and emplacement at about 25–22 Ma was immediately followed by the onset of arc volcanism in Northland [*Rait et al.*, 1991; *Herzer*, 1995]; (4) an eastern unit consisting of Neogene marine sedimentary rocks (megasequence Z) that overlie the allochthon in the east and is faulted against it in the west. Along the Raukumara Range broad Quaternary antiformal uplift up to 4 mm/yr [*Litchfield et al.*, 2007; *Wilson et al.*, 2007] (Figure 1) has been interpreted as a manifestation of sediment subduction and underplating at the base of the crust of the Australian plate [*Walcott*, 1987; *Reyners et al.*, 1999].

[10] It is clear from the geometry of the toe of the frontal wedge today that the subducting margin is undergoing tectonic erosion and subduction of material from the front of the wedge. Multibeam bathymetry, side scan sonar and seismic reflection studies [*Collot et al.*, 1996] indicate that the toe of the margin is indented by 10–25 km to the east of Raukumara Peninsula, relative to regions to the northeast and southwest. This is inferred to be the result of repeated impacts of the large seamounts that are abundant on the northern Hikurangi Plateau. The two most recent impacts have left the major Ruatoria and Poverty indentations [*Lewis et al.*, 1998; *Collot et al.*, 2001] in the margin east of Raukumara Peninsula (Figure 1). Also, immediately to the north of Raukumara Peninsula additional northward traveling debris avalanches have been mapped (Matakaoa Submarine Instability Complex, off Matakaoa Scarp, as part of the Raukumara Plain in Figure 1) where ~3200 km^3 of sediment has accumulated in the last 5 Ma [*Lamarche et al.*, 2008]. These mass transport deposits are likely to be the result of slope oversteepening associated with peninsula uplift and Raukumara Basin subsidence.

3. Seismic Wide-Angle Data Analysis

3.1. Data and Modeling

[11] In March 2007, seismic wide-angle data were acquired onboard R/V *Sonne* as part of the MANGO (Marine Geoscientific Investigations on the Input and Output of the Kermadec subduction zone) project [*Flueh and Kopp*, 2007]. A total of 29 Ocean Bottom Seismometers and Hydrophones(hereafter OBS/H) [*Bialas and Flueh*, 1999] were deployed from about 40 km east of the subduction front on the Hikurangi Plateau, across the deformation front and East Cape Ridge, and covering the eastern part of the Raukumara fore-arc basin (MANGO-1 in Figure 1). Airgun shots from a 64 liter G gun cluster, spaced nominally at 150 m, covered the line of OBS/H stations and extended across the entire Raukumara Basin and ending on the Kermadec Ridge near Whakatane volcano. Adverse weather conditions led to the occasional interruption of the shooting when the ship had to leave track to sail into the wind. The data quality generally is moderate, with signals recorded at offsets up to 30–50 km, and to 70 km in Raukumara Basin.

[12] The seismic wide-angle data were used to generate a two-dimensional (2-D) P wave velocity model of the crust and uppermost mantle using the ray tracing and travel time inversion method of *Zelt and Smith* [1992]. This method calculates arrival times through forward ray tracing in a model that consists of nodes for layer depth and velocities at the top and bottom of each layer. The calculated arrival times are compared to the observed ones and the misfit is reduced either by automatic least squares inversion or by manually adjusting the model. A resolution matrix is calculated to assess the model uncertainty [*Zelt and Smith*, 1992].

[13] Bathymetry data and structure and interval velocities from the coincident seismic reflection profile RAU07-05 (see below) provide prior information and were used to determine the shallow structure for a suitable starting model. The final model was determined from the top down, adding seismic phases with longer offsets from deeper structures. This strategy prevents smearing effects of possibly inaccurate shallow structures into deeper parts of the model. As our preferred final model should only consist of structures derived from the data plus the prior information, the final model is a "minimum parameter/prior structure" model as defined by *Zelt* [1999]. Our modeling involved both automatic inversion and manual model adjustments at complex model regions or limited data coverage where automatic inversion proved difficult.

[14] Examples of the wide-angle data are shown in Figures 2a–2f. Our interpreted P wave phases comprise first and secondary arrival refractions as well as reflections wherever they could be identified. First, we only picked signals of relatively high signal-to-noise ratios, and after a first estimate of the seismic structures, we also picked weaker signals when also observed on coincident multichannel seismic reflection data. The slope of the refracted phases provides an apparent velocity which we used to distinguish between sedimentary, crustal and mantle phases, and the reflections where matched correspondingly. The following seismic phases were picked: (1) refracted arrivals from the sediments (Psed) (e.g., Figure 2a), upper and lower crust (Pg) (e.g., Figure 2b), and uppermost Australian mantle (Pn) (Figures 2e and f); and (2) later arrivals corresponding to reflected waves from intermittent boundaries such as from the presumed decollement (PdP) (Figure 2c), midsedimentary reflection from Raukumara Basin (PsedP) (Figure 2f), and finally deeper reflections from Australian

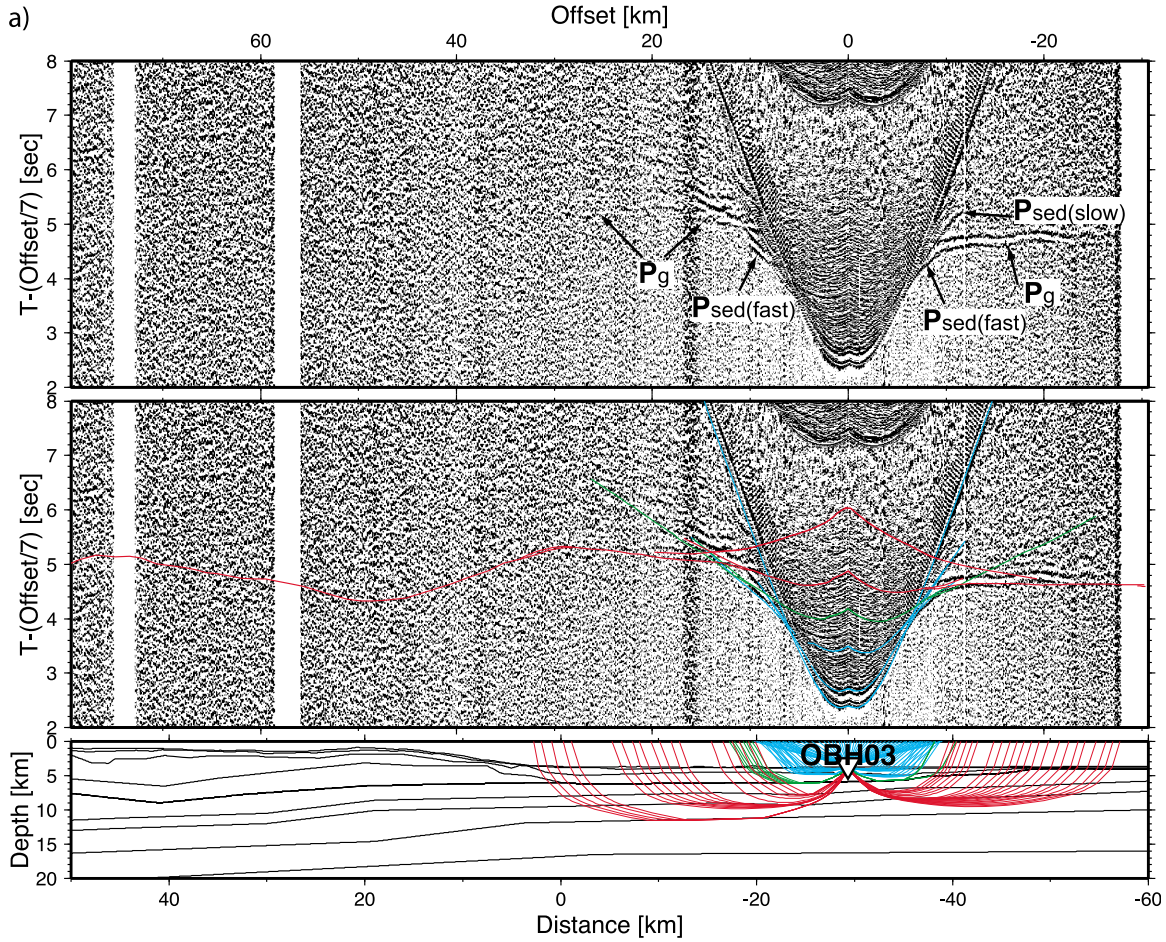

Figure 2. Data examples and predicted arrivals of every fifth OBS/H: (a) OBH03, (b) OBS07, (c) OBS12, (d) OBS15, (e) OBS21, and (f) OBH28. Locations of these example stations are marked in Figure 1. (top) Data with annotated seismic phases. (middle) All predicted P wave arrivals drawn on top of the seismic data, and (bottom) rays for picked arrivals only. Note the contrast in data quality and offset range between western stations on Raukumara Basin (model distance >100 km) and the eastern station on the East Cape Ridge and the Hikurangi Plateau. Annotated seismic phases are as follows: Psed(fast/slow), refraction through (fast/slow) sediments; Pg(u/l), refraction through (upper/lower) crust; Pn, refraction through mantle; Pmv, refraction through shallow high-velocity anomaly (interpreted as Matakaoa volcanics); PdP, reflection from decollement; PsP, reflection from sediments; PcP, reflection from midcrust; PmP, reflection from Moho.

crust (PcP) and Moho (PmP) (Figure 2f) identified in the coincident multichannel seismic reflection profile RAU07-05 (below). We were unable to detect deeper phases from the incoming Pacific plate, and neither could we pick reflections off the downgoing slab beneath Raukumara Basin as these arrivals were masked by the water column multiple (Figure 2f). In total 4400 arrivals were picked and modeled.

3.2. Seismic Velocity Model

[15] Figure 3 shows our preferred final model together with the seismicity of the northern Hikurangi margin. The shallow part below the water layer consists of three continuous sedimentary layers with seismic velocities between 1.6 and 3.6 km/s, covering both the Pacific and the Australian part. The thickness of these layers varies from around 2 km on the incoming plate to about 5 km at 25 km east of East Cape Ridge and also at 50 km west of East Cape Ridge, near the thickest part of Raukumara Basin. In the east and below the three sedimentary layers, the incoming Hikurangi Plateau also includes a 2 km thick layer with seismic velocities of 3.8–4.0 km/s which thickens under East Cape Ridge to form a 10 km thick and 20 km wide high velocity zone. As discussed below, this layer is not likely to represent a single geologic unit but allowed a simpler velocity model. The Hikurangi Plateau crust consists of three crustal layers of which the uppermost layer only marks a change in the velocity gradient of the shallow crust. The upper crust is about 4 km thick with seismic velocities from 4.9 to 6.7 km/s, and the uppermost lower crust has a velocity of about 7.1 km/s. Note that the Moho shown below the 10 km thick Hikurangi Plateau is based on the gravity modeling (below) and is not resolved by the seismic data.

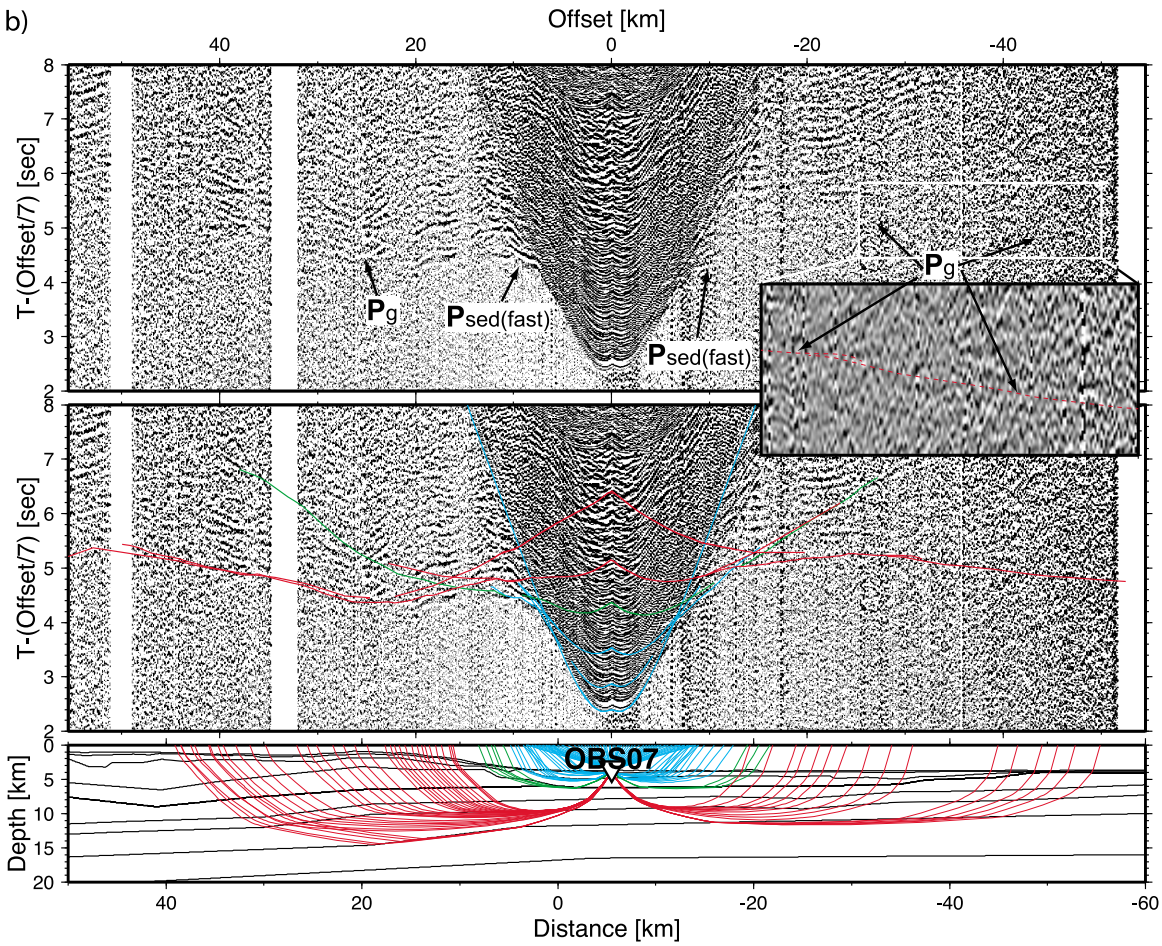

Figure 2. (continued)

[16] West of the trench, the fore arc has an additional sedimentary layer below the three shallow ones, with a maximum thickness of up to 5 km but thinning considerably below East Cape Ridge and also towards Kermadec Ridge to the west, with seismic velocities between 3.7 and 3.9 km/s. The Raukumara basin structures were modeled as five layers. The deepest layer has relatively fast seismic velocities of 4.6–4.9 km/s, is on average about 3 km thick, and manifests a maximum depth of 12 km for Raukumara Basin. The Australian arc crust was modeled as two crustal layers, with seismic velocities of 5.4–5.8 km/s and 6.5–6.8 km/s, respectively, forming an about 5 km thick crust below and east of the thickest part of Raukumara Basin, and thickening to approximately 10 km to the west. Finally, the uppermost Australian arc mantle has a seismic velocity of 8.0–8.1 km/s. Details of the model features are discussed below.

[17] The data examples in Figures 2a–2f also show predicted arrival times from our preferred final model. Figures 2a–2f (middle) show all predicted P waves plotted on top of the recorded data, whereas Figures 2a–2f (bottom) only shows rays that correspond only to the picked arrivals to indicate model coverage. The average RMS misfit of the predicted arrivals is 70 ms which, taking into account the relatively large data uncertainty from the reduced data quality, corresponds to a normalized chi-square value of just below 1.

[18] Model resolution and coverage are shown in Figure 4, using only the seismic wide-angle reflection and refraction data without taking into account available multichannel seismic (MCS) data (see below). Resolution values between 0.0 (small symbols) and 1.0 (large symbols) indicate how well each model parameter is resolved with respect to the relative number of rays. *Zelt and Smith* [1992] found that a node with a resolution value greater 0.5 is considered well resolved. Evaluating model resolution together with the ray paths, Figure 4 shows that the shallow structures of the Hikurangi Plateau are well resolved. In the central part, below East Cape Ridge, only few rays could be traced and used for determining the deeper structure, yet the shallow structures again appear well resolved. Raukumara Basin in the west is well resolved in its central part down to the arc mantle at 19 km depth, although its western part is increasingly less resolved by the wide-angle data. Note that the two layers defining the Australian crust have, for simplicity reasons, each a single upper velocity node at the western edge of the model. Therefore, the velocity resolution values of these two nodes, though outside the ray coverage, are relatively large due to the ray coverage from

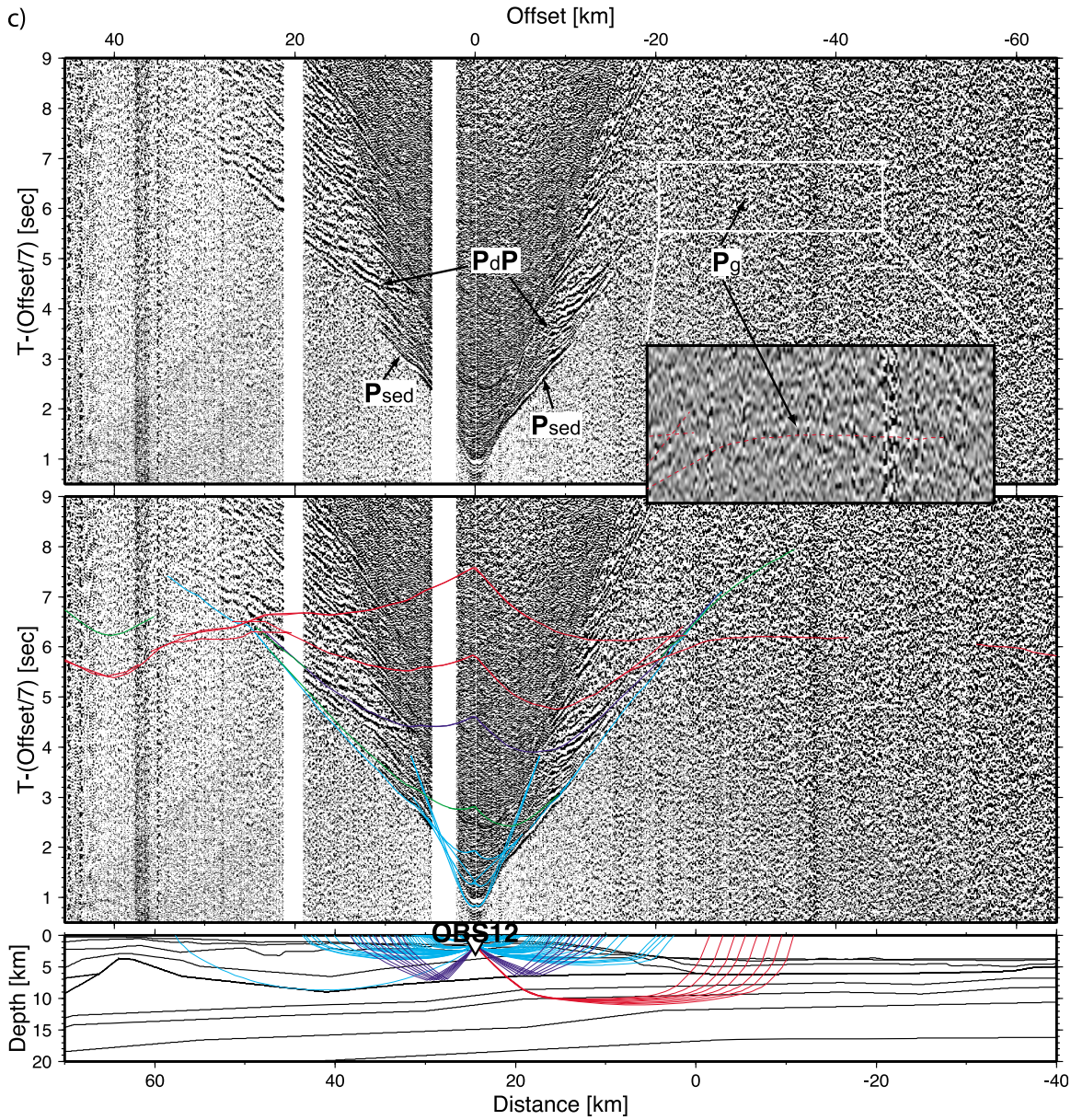

Figure 2. (continued)

the center of Raukumara Basin. The structures of the western Raukumara Basin are entirely based on the MCS data as shown below, and no modeling emphasis has been placed to this region outside the OBS/H station distribution. The MCS data are also the basis for modeling the shallow sedimentary structures and therefore the resolution of the high number of model nodes is not shown here. Similarly, the subducting slab is manifest as a bright reflector in the MCS data and was used to determine the slab dip below Raukumara Basin but is not visible in the wide-angle data.

[19] In order to estimate model uncertainties, we performed predominantly a trial and error sensitivity study of model parameters and examined the resulting RMS misfit. The best fit average RMS value of 70 ms, corresponding to a chi-square value of about 1, increased to levels of 100–150 ms (chi-square around 2–4) which were deemed too large, thus providing a range of suitable model parameters that still fit the data. In addition, we took into account the results provided by the RAU07 MCS data (below) and stacking velocity data determined by normal moveout velocity analysis (Figure S1).[1] Since the streamer length used in acquiring the MCS data was 7.3 km, these data provide independent constraint on the upper crustal velocity structure. The variability between travel time and depth, relative to the seabed, is shown in Figure S1, where the mean velocity depth curve (red) is compared to the velocity structure at model distance 150 km (superimposed in blue). Using these data the location of the westernmost OBH station (model km 126), the base of the upper two sedimentary

[1] Auxiliary materials are available in the HTML. doi:10.1029/2009JB006645.

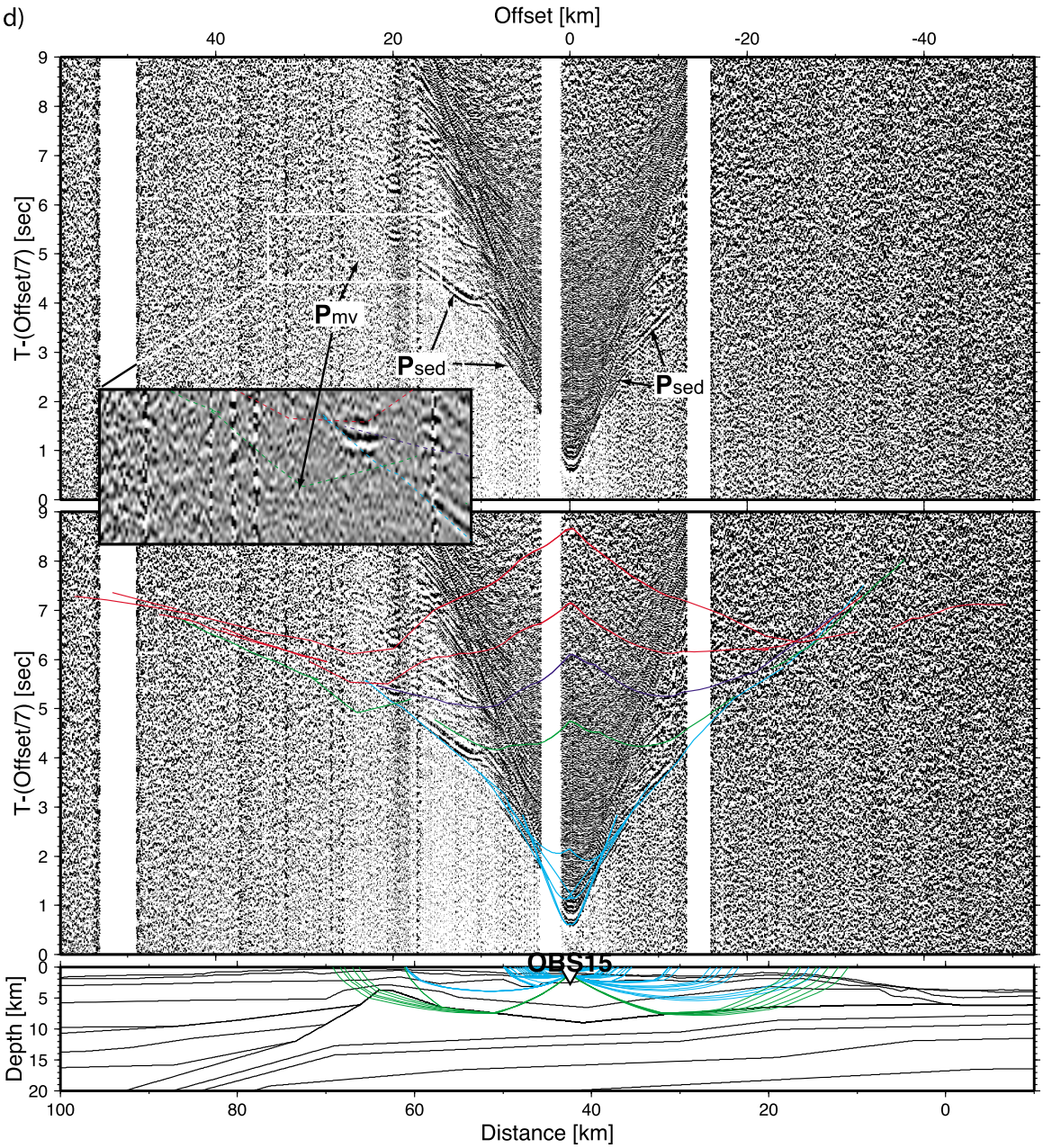

Figure 2. (continued)

layers (megasequence Z after *Sutherland et al.* [2009]) at 4.6 s two-way travel time (TWT) converts to 4.25 km depth, using stacking velocities, compared to 4.21 km depth in Figure 3. The interval velocity immediately above the reflector is 3.17 km/s and 3.04–3.20 km/s in the MCS and wide-angle results, respectively. Similarly, at the same location, the base of the sediments (megasequence Z, *Sutherland et al.* [2009]) at 8.4 sec TWT converts to 11.40 km (interval velocity above: 4.6 km/s) in the MCS data, compared to 11.80 km depth (velocity above: 4.6–4.9 km/s) in Figure 3. Another comparison comes from earthquake tomography immediately to the south of our working area [*Reyners et al.*, 1999], where mid- and lower crustal velocities between 5.0 and 7.5 km/s compare reasonably well with our estimates of 5.4 to 7.2 km/s. Note, however, that some parts of the model remain relatively poorly resolved, for example beneath East Cape Ridge the data penetration was reduced by scattering and attenuation. In areas without OBS/H coverage (model edges) or where ray coverage is limited the velocity model is not constrained. Given the above discussion, and considering model ray coverage and node resolution the following model uncertainties are estimated (larger estimates in brackets are for deeper or less resolved structures): Depth to sediments: ±80 (300) m; depth to crust: ±100 (500) m, depth to mantle:

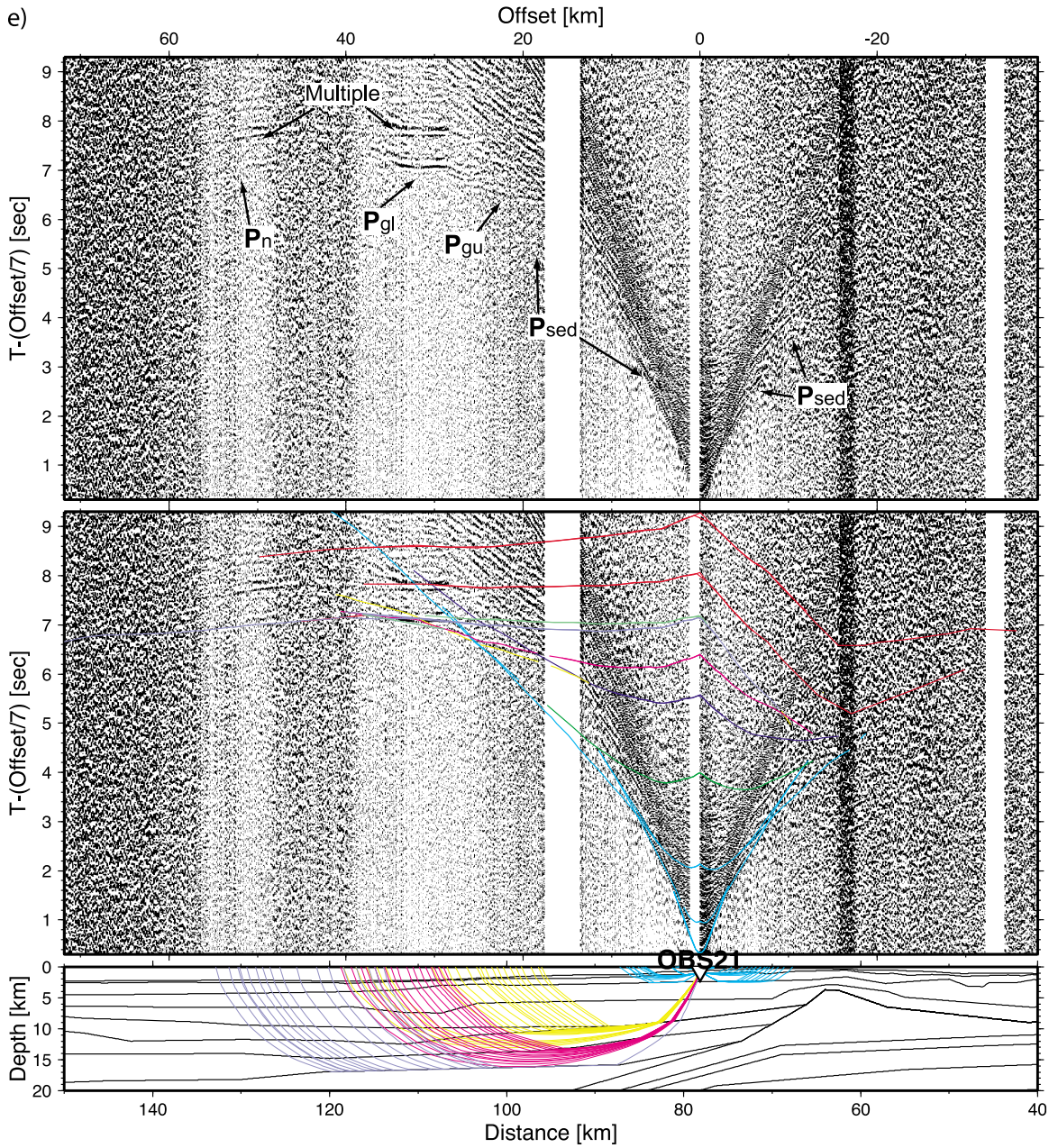

Figure 2. (continued)

±500 (1000) m; velocity of sediments: ±100 (300) m/s; velocity of crust 80 (400) m/s; velocity of mantle: ±150 m/s.

4. Coincident Seismic Reflection Profile

[20] The wide-angle reflection and refraction line MANGO-1 was colocated with the MCS line RAU07-05, which was recorded also in 2007 several months after the MANGO-1 deployment [*Sutherland et al.*, 2009]. Data for RAU07-05 were acquired using a 86.5 l (5280 cu in) source and 7.3 km streamer, with 50 m shotpoint spacing and 15.3 s record length. The data were processed in a conventional manner (including several filters and deconvolution) with an emphasis on multiple attenuation up to a prestack time migrated section (Fugro Seismic Imaging, Raukumara Basin 2-D seismic survey (RAU07), New Zealand, unpublished report, pp. 1–37, Ministry of Economic Development, Wellington, 2007, see also Table S1).

[21] Figure 5 shows an uninterpreted as well as an interpreted version of line RAU07-05. The interpreted version also shows the wide-angle model drawn as reflections in two-way travel time (TWT) on top. Following the interpretation of *Sutherland et al.* [2009], the reflection strata can be divided into three sedimentary megasequences, X, Y, and Z, (Figure 5) which were put into context by correlating them with the surrounding geology including what has been mapped onshore. Starting from the top, megasequence Z is the upper band of continuous or semicontinuous reflections

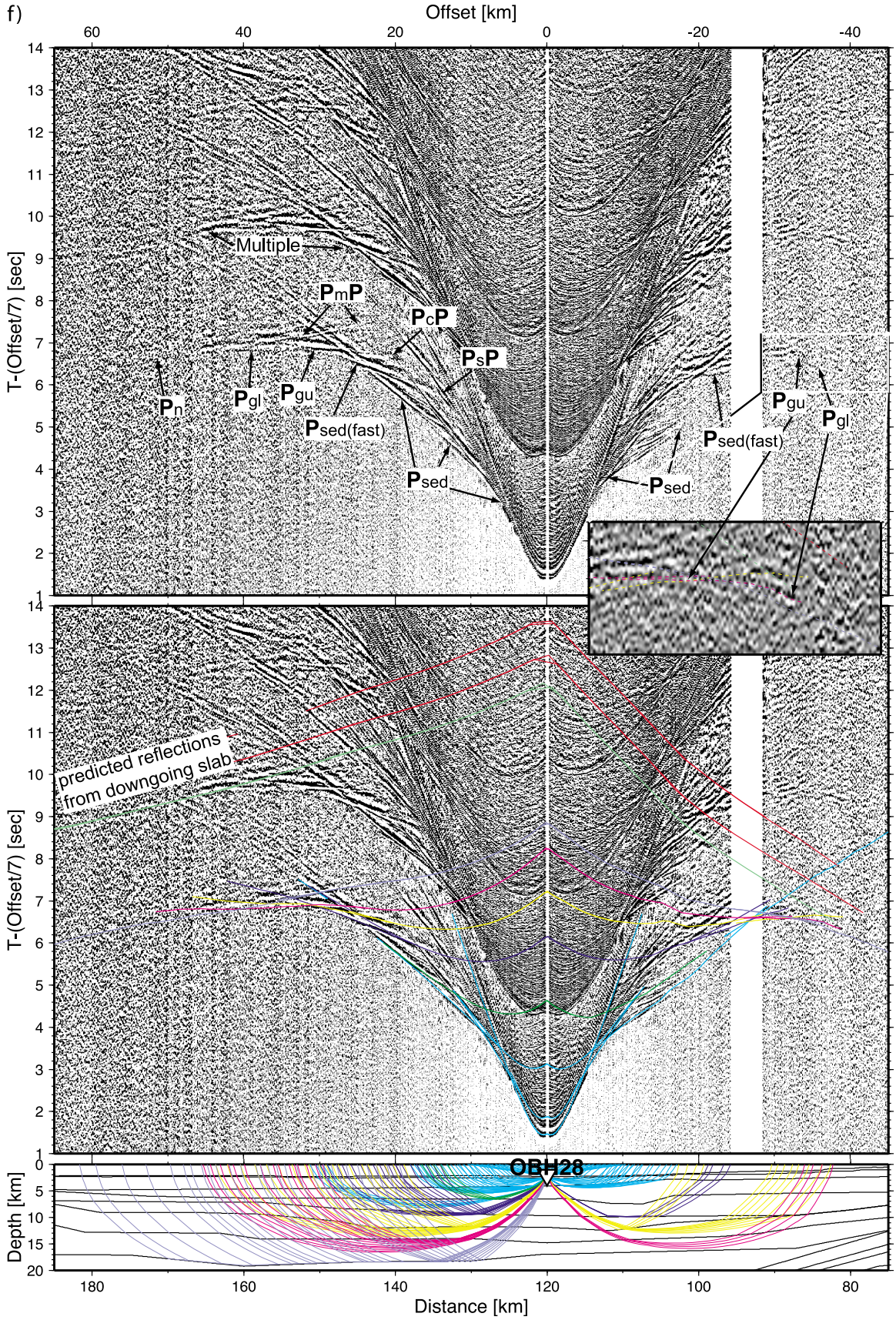

Figure 2. (continued)

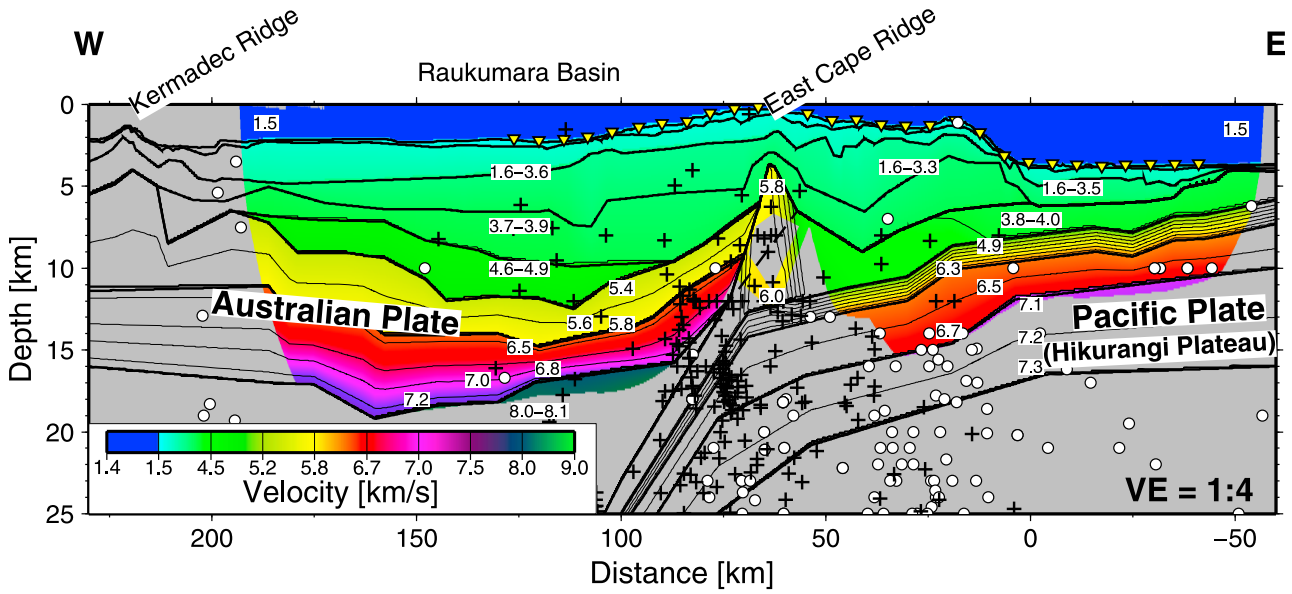

Figure 3. Final proposed velocity model derived from ray tracing of the seismic wide-angle data. Masked areas represent parts of the model without ray coverage, though seismic reflection data from line RAU07-05 as well as gravity data were used to place some constraints on this model as explained in the text. Also shown are earthquakes from the global database with magnitudes larger than 4 from within 50 km of either side of the model (circles) and from the Raukumara Peninsula network from *Reyners et al.* [1999] from up to 100 km to the south of our profile (crosses). Note the increased concentration of hypocenters around the location where the incoming plate bends most below the fore arc.

comprising recent slumps and slides including the Matakaoa Submarine Instability Complex across the Raukumara Plain [*Lamarche et al.*, 2008] as well as the downslope collapse structures east of East Cape Ridge [*Sutherland et al.*, 2009]. The bottom of megasequence Z is marked in our model as the bottom of the second sedimentary layer, reaching down to 4.5 km depth (2.5 km below seafloor) around model km 185, the depocenter of the more recent arc volcanic input. The base consists of mostly continuous reflectors [*Sutherland et al.*, 2009].

[22] Megasequence Y is a thin unit (0–1.6 km thick) of chaotic and variably dipping reflections extending between East Cape Ridge and the center of Raukumara Basin where it pinches out [*Sutherland et al.*, 2009]. Due to its small size, however, we did not include a small additional layer in our model (Figure 3) but combined this unit with our sedimentary layer 3. Megasequence Y is interpreted to represent a single large Cenozoic allochthonous slope failure originating from East Cape Ridge [*Sutherland et al.*, 2009].

[23] The underlying megasequence X is another band of continuous or semicontinuous reflections below megasequence Y and is up to 8 km thick in the deepest part of Raukumara Basin [*Sutherland et al.*, 2009]. The sedimentary strata are interpreted to correlate with Cretaceous onshore deposits and appear to be remarkably little deformed considering its age and the tectonic history of the region [*Sutherland et al.*, 2009].

[24] Below the sedimentary megasequences there appear clear reflections from the top of the Australian crust and the Moho, indicating the thinning of the crust around model km 110. The high amplitude sub-Moho reflection at 15 s TWT around model km 130 is interpreted and modeled as the top of the downgoing slab (Figure 5).

[25] In contrast to the relatively deep reflectivity within and beneath the Raukumara fore-arc basin, the MCS profile reveals a relatively unreflective outer fore-arc high (East Cape Ridge), indicating intensive fore-arc deformation potentially destroying coherent reflectivity here. The interpreted decollement reflection that appears on the seismic wide-angle data (PdP on Figure 2c) would be predicted on the MCS data around model km 25 at about 5.5 s TWT but does not appear as a high amplitude reflection here. Furthermore, the incoming Hikurangi Plateau appears also relatively unreflective, probably due to its rough, seismically scattering crust or its weakly reflective internal composition. Further discussion is given below.

5. Gravity and Magnetic Data and Modeling

[26] Potential field data from ship measurements along our profile were used to verify and improve the seismically derived structural model as well as to constrain seismically unresolved sections of the model. In particular, gravity data helped to estimate the thickness of the incoming Hikurangi Plateau, where no deep mantle phases could be identified in the seismic data. The magnetic anomalies yielded information on the occurrence of volcanic rock type and origin.

[27] For an overview, Figure 6 shows a 3-D view of gravity and magnetic anomalies draped over the bathymetry. The 3-D gravity anomalies stem from satellite data [*Sandwell and Smith*, 1997]. The magnetic grid is a compilation of aeromagnetic data [*Malahoff et al.*, 1982] and all available

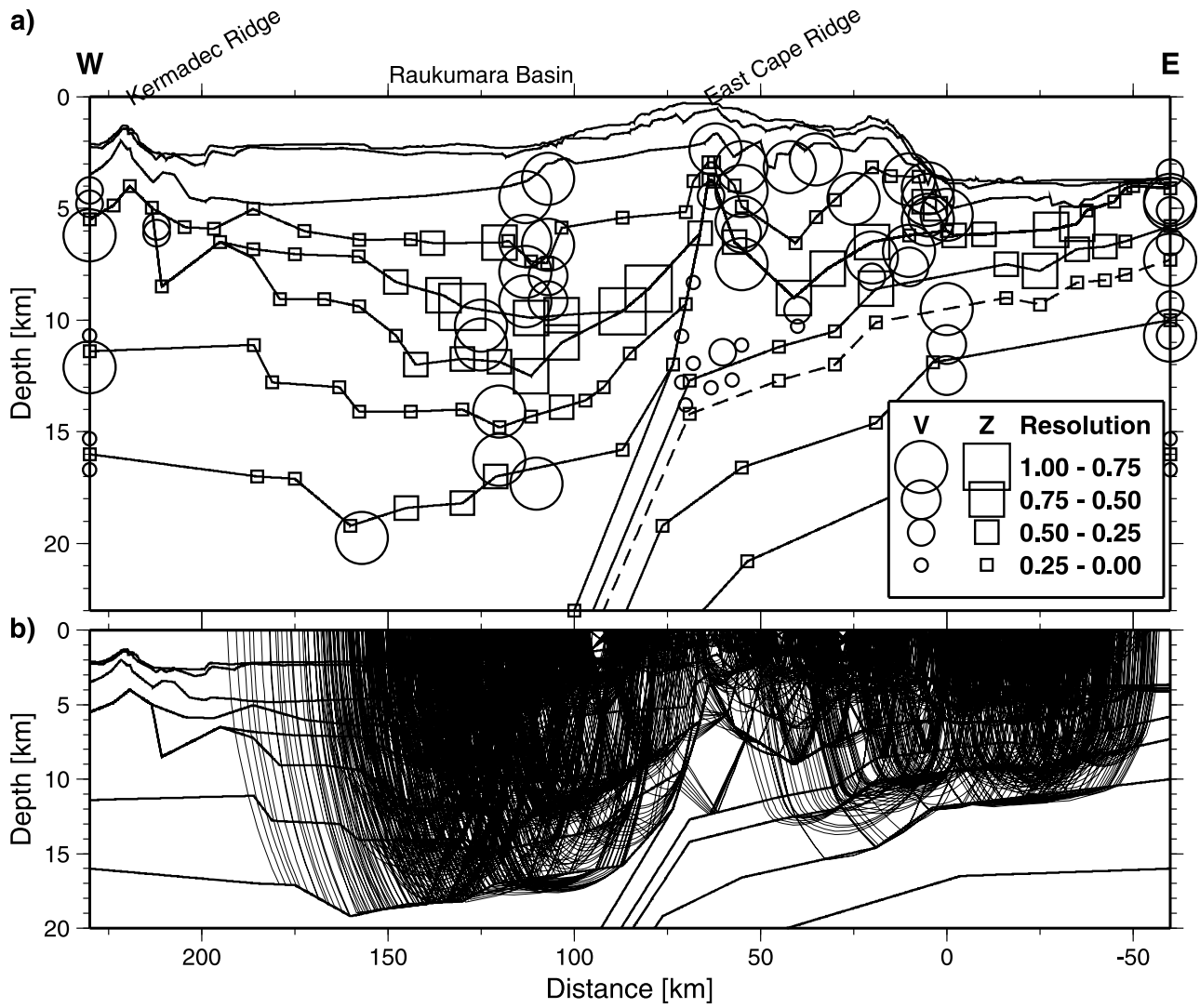

Figure 4. (a) Model resolution, with depth nodes (squares) and velocity nodes (circles) drawn to scale indicating node resolution; values larger than 0.5 are considered well resolved. (b) Model coverage, demonstrating the shallow coverage of the incoming Hikurangi Plateau and comparably good coverage of the Raukumara Basin structures. The gap in the center is due to relatively weak seismic signals recorded to relatively narrow offsets, probably caused by high seismic attenuation within the margin wedge of the fore arc.

ship data from the region, including newly collected data from the seismic cruises in 2007, leveled to a common surface.

[28] The most notable feature in the gravity data is the −140 mgal gravity low at the southern part of Raukumara Basin. This gravity low is associated with both the deep basin as well as the southward thickening of the Australian Plate during its transition from island arc to continental character.

[29] The magnetic field exhibits distinct positive (>150 nT) anomalies extending from the Matakaoa volcanic anomaly onshore northeastward along East Cape Ridge (Figure 6). This corroborates the suggestion by *Davey et al.* [1997] that the magnetic anomalies along East Cape Ridge are associated with the same allochthonous material as observed onshore.

[30] Gravity and magnetic data were also acquired along with the seismic reflection data of line RAU07-05. Along MANGO-1 the observed potential field data (Figure 7) were modeled using Encom's ModelVision™ software and a 2.5D geometry for each layer. The lateral extent in and out of the model plane of the deeper parts of Raukumara Basin was limited to ±50 km in accordance with the seismic reflection data [*Sutherland et al.*, 2009]. In constructing our gravity and magnetic models we used the velocity structure from wide-angle seismic data (Figure 3), all available data from samples of equivalent rocks exposed onshore, and previous interpretations of potential field data along the Hikurangi margin [*Gillies*, 1984; *Davy and Wood*, 1994; *Davey et al.*, 1997; *Davy et al.*, 2008; *Sutherland et al.*, 2009]. Oceanic crust of the Hikurangi Plateau is assumed to consist of a basaltic upper crust (2.85 g/cm^3, magnetic

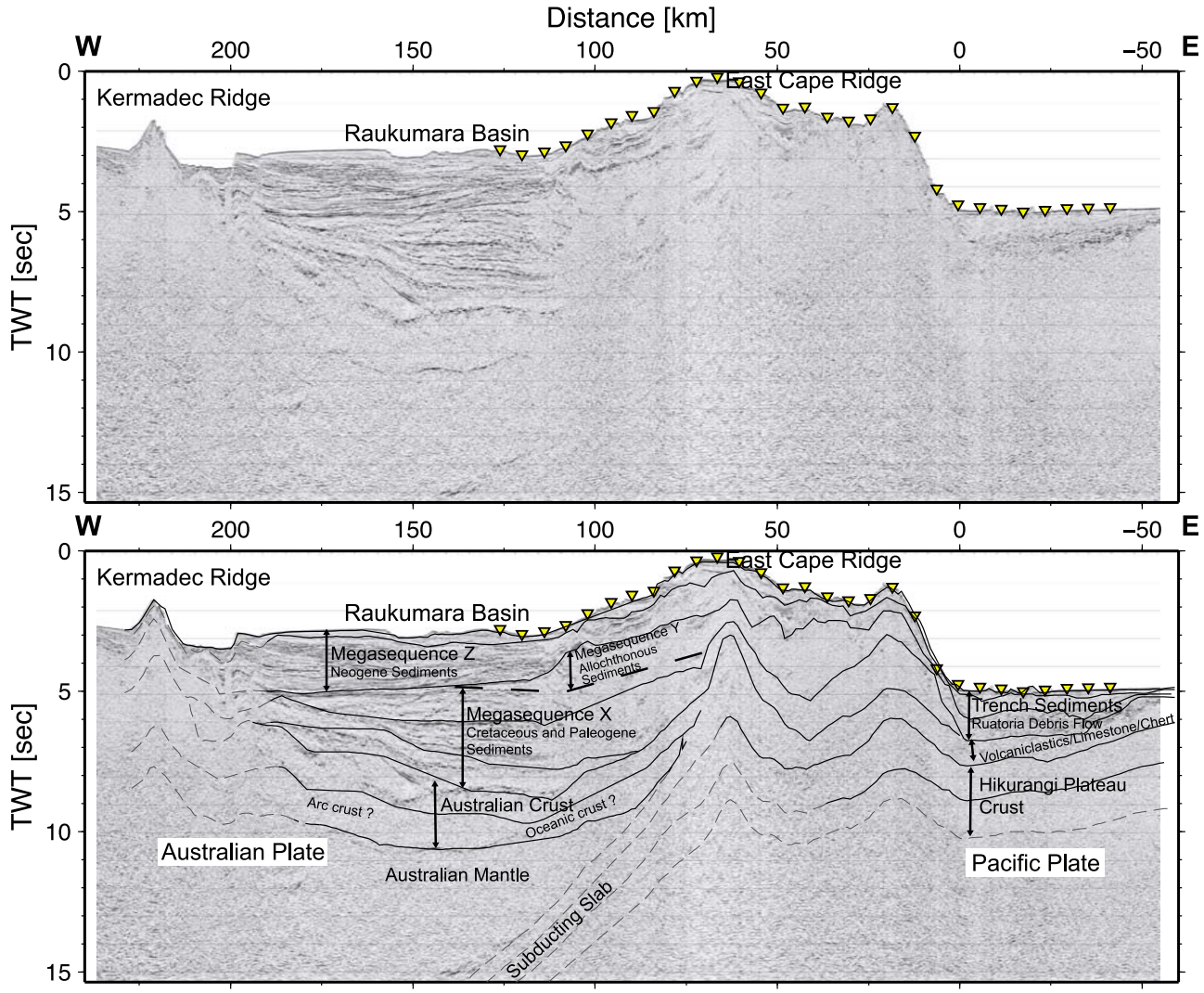

Figure 5. Seismic reflection data from line RAU07-05 in migrated form. (top) Without and (bottom) with velocity model structures (converted to two-way travel time (TWT)) and also the interpretation by *Sutherland et al.* [2009] overlain. Dashed reflectors are not resolved by the seismic wide-angle data. Triangles on seafloor mark OBS/H stations. West of the stations, the velocity model does not predict the reflections well, as no modeling emphasis was placed outside the region of wide-angle data coverage (Figure 4).

susceptibility 0.02) underlain by denser gabbro and metagabbro (3.15 g/cm^3, magnetic susceptibility 0.05) and a mantle density of 3.4 g/cm^3. Below the base of the reference lithosphere (at 70 km depth) a density anomaly was inserted to model the subducting plate lithosphere sinking into the asthenosphere. The lower crust of the North Island is assumed to be comprised of metamorphosed greywacke rocks (2.75 g/cm^3) overlying denser amphibolite and granulite (3.05 g/cm^3, magnetic susceptibility 0.05). The oldest sediments in the Raukumara Basin are assumed to have a density of 2.6 g/cm^3 and the younger basin fill has densities of between 2.2 and 2.3 g/cm^3. Compared with *Sutherland et al.* [2009] the model density values in Figure 7 are about 5–10% denser in the lower parts (except for the mantle) but up to 5% lighter in the shallower parts of the model. The latter discrepancy can readily be explained by the simplicity of *Sutherland et al.*'s [2009] density model which aimed at providing a consistency between the general structural interpretation and the observed densities without taking into account the accuracy of our new seismically derived crustal velocity model. While, the velocity model provides some constraints on the gravity model, alternative thicknesses of the upper and lower crust and Hikurangi Plateau are possible. For example, allowing up to 10% variations in crustal densities results in a total crustal thickness uncertainty of ±5 km. The uncertainty in the thickness of the Hikurangi Plateau from gravity models is estimated to be ±4 km [*Davy and Wood*, 1994].

[31] The magnetic anomalies proved more difficult to be modeled in 2-D and we expect much of the existing misfit to be due to 3-D effects. Our main aim here was to determine the cause of the two major positive anomalies; one at the western edge of the model, coincident with the Whakatane volcano, and the second being the East Cape Ridge anomaly

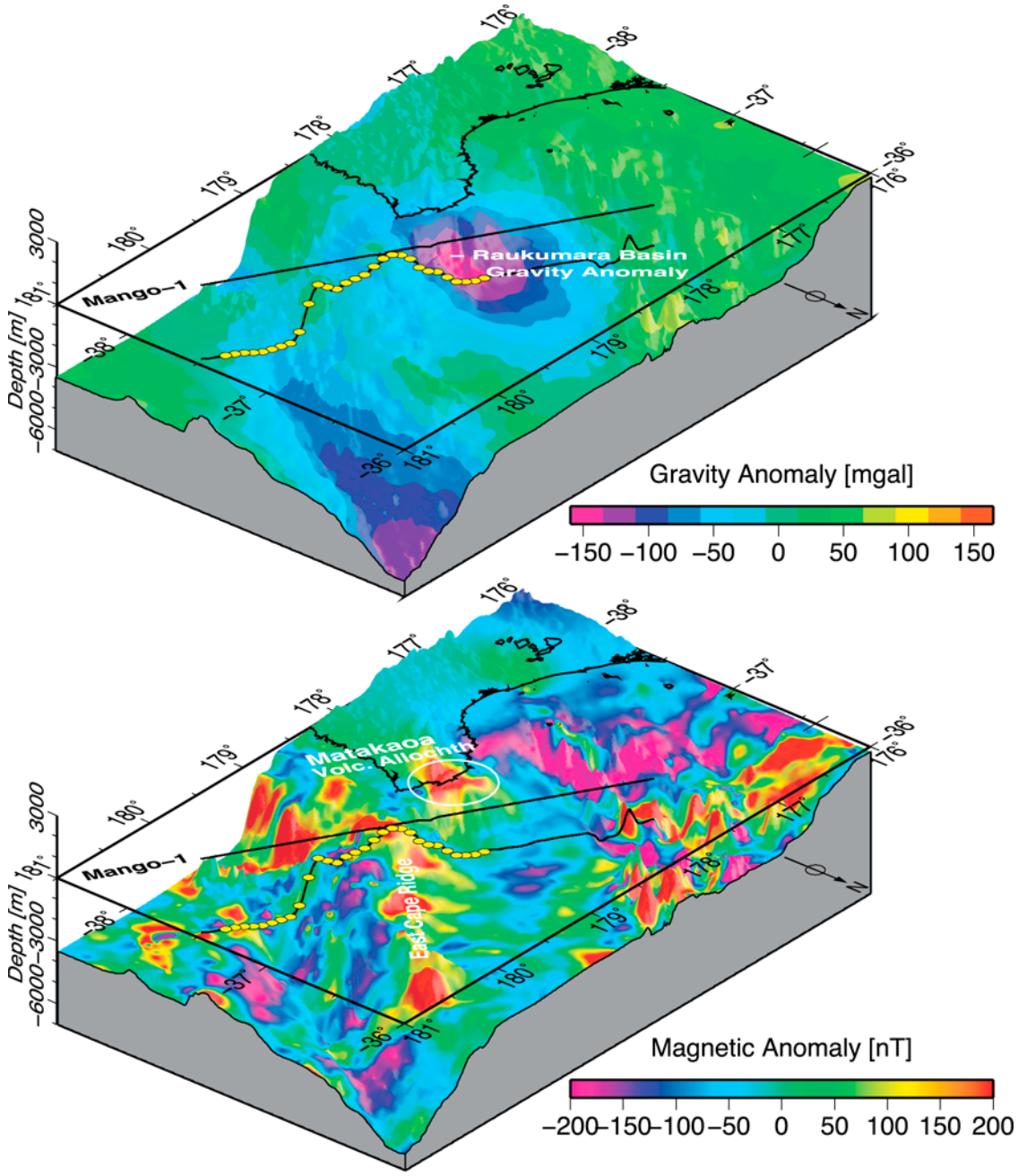

Figure 6. Gravity and magnetic data around the northern Hikurangi margin, viewed from northeast. (top) Gravity data reveal a prominent –140 mgal anomaly associated with Raukumara Basin. (bottom) East Cape Ridge exhibits several large magnetic positive anomalies that can be traced towards land to link up with the Matakaoa volcanics.

at model km 65. Both can be modeled by highly magnetized uppermost crust. The highest magnetic susceptibilities used were 0.085 to 0.1 and convert to magnetizations of 3.3 to 3.9 A/m. These values are larger than the largest magnetizations of up to 3.3 A/m used by *Davey et al.* [1997] but within the range of magnetizations (1.0 to 4.5 A/m) used by *Gillies* [1984], who had a more localized distribution of magnetic sources. By assigning low magnetizations to the remaining layers (magnetic susceptibility <0.05, magnetization <2.0 A/m), magnetic anomalies of similar magnitudes and wavelengths as the observed anomalies are produced. A detailed distribution of magnetic sources [*Gillies*, 1984; *Davey et al.*, 1997] to more accurately fit the observed data goes beyond the purpose of our interpretation as discussed below.

[32] A second magnetic model was produced using 2-D Euler deconvolution which uses the gradients of the magnetic anomalies to invert for source depths and location [*Durrheim and Cooper*, 1998; *Cooper*, 2002, 2004]. Figure 8 shows the most likely distribution of magnetic sources along the model. The result matches the East Cape Ridge anomaly relatively well and corresponds to the high magnetic sus-

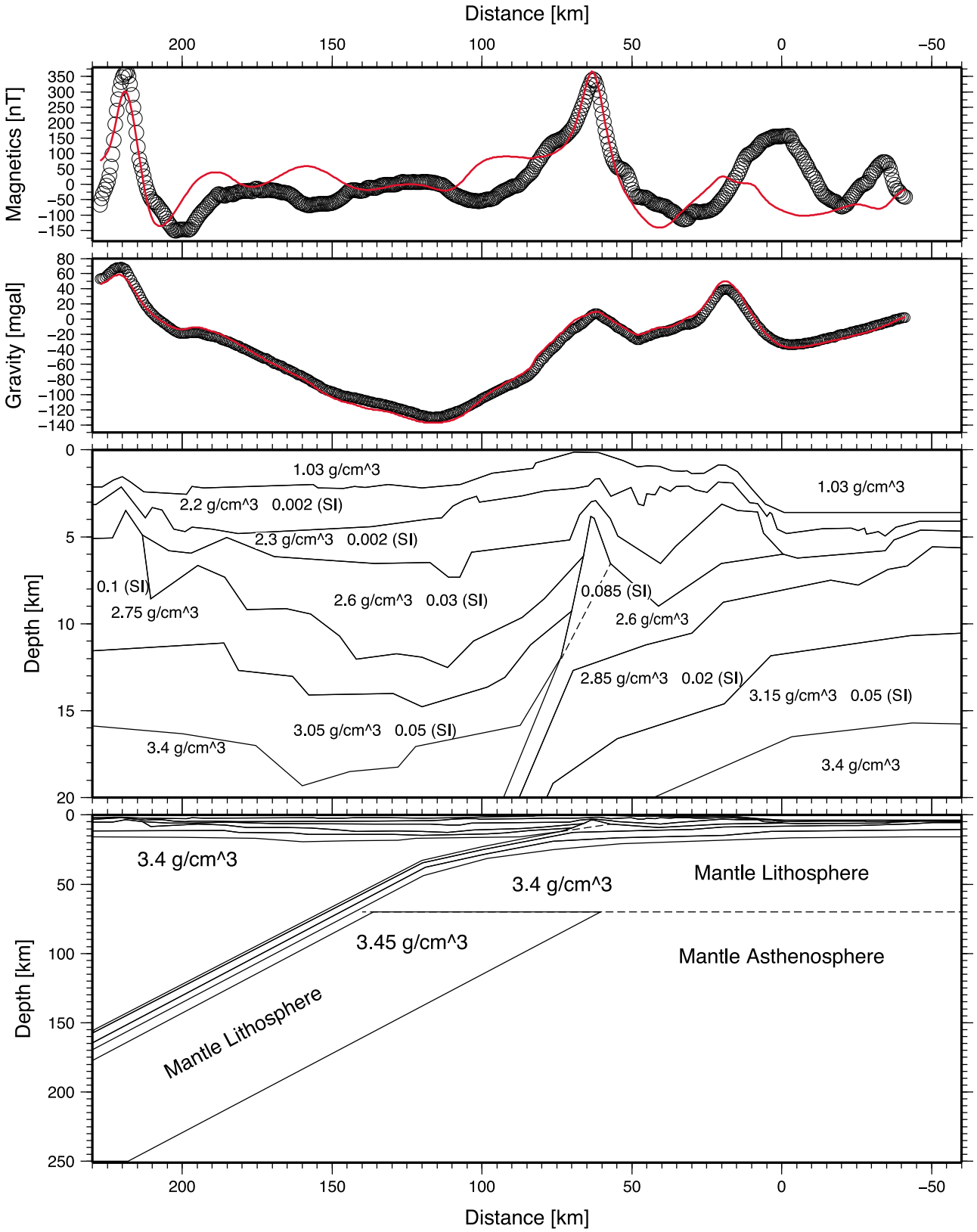

Figure 7. Gravity and magnetic model from 2.5-D modeling. Model layers extend practically indefinitely in all directions except the deep sedimentary layer in Raukumara Basin which was limited to 50 km in and out of the model plain. Densities are given for all layers, magnetic susceptibility (dimensionless number behind density) is given only for magnetized layers.

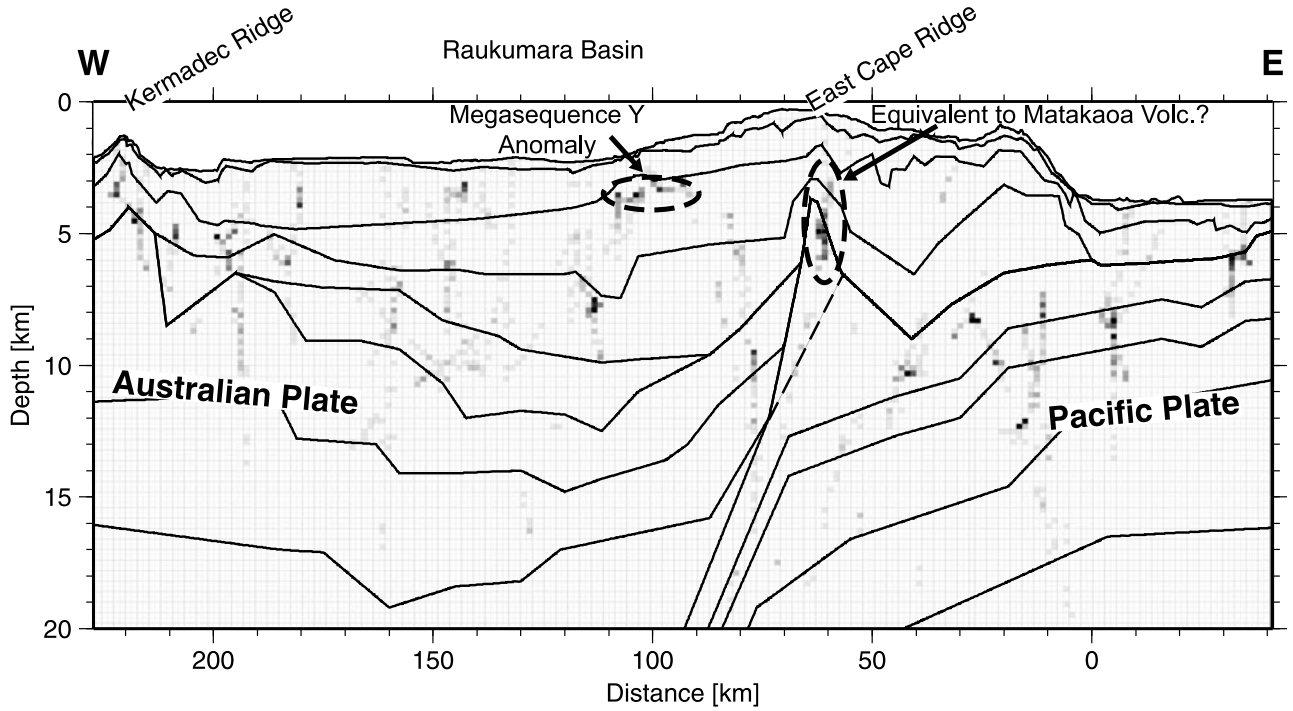

Figure 8. Magnetic Euler deconvolution, indicating regions for likely magnetic sources. Black marks most likely, gray marks likely, and white marks unlikely locations for magnetic sources. Note the reasonably good correlation of the East Cape Ridge anomaly of the seismic velocity structure (drawn on top). Also remarkable are the shallow anomalies at the eastern edge of Raukumara Basin, which are associated with the large slump called megasequence Y [*Sutherland et al.*, 2009], originating from the East Cape Ridge anomaly.

ceptibility body (0.085, magnetization 3.3 A/m) identified in Figure 7. But, Euler deconvolution fails to focus magnetic sources at the western model edge (Whakatane volcano) where the deconvolution window cannot capture the full wavelength of the associated magnetic anomaly. Another interesting area of magnetic sources occurs around model km 100, at about 3.5 km depth. The source coincides with the thinned frontal edge of part of the offshore allochthon (megasequence Y) as interpreted by *Sutherland et al.* [2009]. The implications are discussed below.

6. Discussion

6.1. Structure and Sediment Cover of the Subducting Hikurangi Plateau

[33] When plateaus enter subduction zones, their role in the subduction processes is manifold. Plateaus such as the Hikurangi Plateau carry a significant amount of water into the subduction zone, potentially leading to voluminous arc volcanism [*de Ronde et al.*, 2007]. Furthermore, plateau crust is usually more buoyant than normal oceanic crust and may therefore cause either subduction erosion [*von Huene and Scholl*, 1991] or enhanced uplift of the fore arc [*Collot and Davy*, 1998; *Kopp et al.*, 2006]. If its thickness is too buoyant for subduction it may halt volcanism [*McGeary et al.*, 1985] or actually stall subduction entirely [*Cloos*, 1993; *Mann and Taira*, 2004; *Davy et al.*, 2008]. Our results place some new constraints on the geometry of the subducting Hikurangi Plateau.

[34] The northern Hikurangi Plateau is modeled as a 10 (±1) km thick crust (Vp > 4.9 km/s) that is overlain by up to 4 km of seismically slow (<4.0 km/s) material (Figure 3). We interpret the topmost 2.2 (±0.1) km of sediments with seismic velocities increasing from 1.6 to 3.5 km/s to consist of predominantly coarse debris sourced by the collapsing frontal slope (e.g., Ruatoria Slide, Figure 1). Below that lies a 2 (±0.2) km thick layer with seismic velocities of 3.8–4.0 km/s which, following the recent description of the Hikurangi Plateau by *Davy et al.* [2008], is a mixed layer of volcaniclastics, limestone, and chert (Figures 5 and 9). This interpretation is based on the seismic velocities (too slow for basaltic or gabbroic crust) which are near the faster limit of volcaniclastics, dredged from adjacent to the survey area [*Hoernle et al.*, 2004], and limestone and chert as sampled by drill cores from similar oceanic plateaus in the southwest Pacific [*Davy et al.*, 2008].

[35] Where the plateau enters the fore-arc, high-amplitude reflections are observed on OBS 12 around 4.5 s (see ray diagram in Figure 2c), and these also appear on the two surrounding OBS. High amplitude reflections above the downgoing plate typically stem from the decollement with elevated pore fluid pressures in the subduction channel below [*von Huene et al.*, 2004]. Our model predicts a suitable reflection (Figure 2c) off a simple continuation of the mixed layer of volcaniclastics, limestone, and chert that produced clear first arrival refractions on the seismic record from the Hikurangi Plateau (Figures 2a and 2b). However, we cannot exclude the possibility that some of the overlying

sediments are carried within this subduction channel. In any case, if our interpretation of these high amplitude reflections is correct, we can infer that at about 20–40 km from the deformation front a subduction thrust occurs at about 7–8 km depth, below a 5–7 km thick hanging wall (Figure 9).

[36] The underlying plateau crust is divided into two layers. The upper 4–5 km thick layer displays seismic velocities of 4.9–6.7 km/s, around the typical average of 5.5 km/s for flood basalts normal for the upper plateau crust [*Coffin and Eldholm*, 1994]. The lower crust could only be detected by a few refractions of a velocity >7.1 km/s, again typical for lower plateau crust that presumably consists of gabrroic to ultramafic material [*Coffin and Eldholm*, 1994]. As no refractions could be detected from the bottom of the plateau, its thickness could only be estimated using gravity data. In our model, the depth of the Moho increases from 16 km in the east to 22 km below East Cape Ridge, yielding a plateau thickness of roughly 10 km. This value appears to be a relatively thin compared internationally to other Large Igneous Provinces (LIPs) with typical thicknesses of 20–40 km [*Coffin and Eldholm*, 1994]. Even compared to previous Hikurangi Plateau estimates of up 23 km thickness for the southern area [*Davy et al.*, 2008] it seems relatively thin, but is in good agreement with other estimates from the central and northern part of this plateau [*Henrys et al.*, 2006; *Davy and Wood*, 1994], and is sufficiently thin to subduct [*Cloos*, 1993].

[37] Subduction of the Hikurangi Plateau occurs at a relatively shallow dip angle of a few degrees up to East Cape Ridge and then appears to steepen downdip. Reflections off the slab as recorded on MCS line RAU07-05 (Figure 5) suggest that the slab dips at around 20° below Raukumara Basin, about 120 km from the deformation front, and deep seismicity indicates an angle of almost 50° further downdip toward the arc.

[38] No direct evidence has been found for the downdip extent of the Hikurangi Plateau, below which the Pacific Plate subducts as normal oceanic crust. Our gravity model (Figure 7) requires less negative density anomalies below the well-imaged Raukumara Basin; as a result we reduced the thickness of the downgoing Pacific plate in this region. This complies with previous notions from tomographic results from Raukumara Peninsula [*Reyners et al.*, 2006] or geometrical considerations regarding the possible common history of the Hikurangi and the Manihiki and Ontong-Java Plateaus [*Davy et al.*, 2008].

6.2. Arc and Fore-Arc Raukumara Basin

[39] The basin stratigraphy of line RAU07-05 has been described briefly above and in length by *Sutherland et al.* [2009] and is shown in Figures 5 and 9. We generally note a good correlation between what has been interpreted as Cretaceous sedimentary units and relatively fast (3.7–4.9 km/s) seismic velocities at depths between 6.0 km and 12.5 km. With an assigned density optimum of 2.6 g/cm^3 these basal sediments are considered to be highly consolidated and weakly metamorphosed. Whakatane volcano of the active Kermadec arc is resolved and detected by the seismic reflection line RAU07-05 and the potential field data (but not the seismic wide-angle data) at model km 220 (Figures 1, 3, 5, and 7–9), at the western margin of Raukumara Basin.

[40] With a sedimentary infill of more than 10 km, Raukumara Basin is one of the deepest known fore-arc basins at an active margin. A comparable fore-arc basin is found at the Middle American subduction zone, Sandino Basin offshore Nicaragua with an infill of up to 16 km [*Ranero et al.*, 2000; *McIntosh et al.*, 2007]. For Sandino Basin it has been suggested that it was created when a new subduction zone developed seaward of the previous (Jurassic/Cretaceous) subduction zone [*Walther et al.*, 2000]. This is strikingly similar to the interpretation in our study area [*Sutherland et al.*, 2009], and perhaps the only mechanism that allows for the development of such superdeep fore-arc basins.

[41] A correlation exists between the thickest and deepest part of Raukumara Basin and the thinnest part of the underlying crust. Below Raukumara Basin, the crustal thickness varies between up to 10 km in the west and as thin as 5 km toward the central and eastern part of the basin (Figure 3). Isostacy would have caused a natural depression at the thinnest part of the crust where sedimentation commenced at the Gondwana margin. With the eastern margin of the basin tilted upwards at East Cape Ridge, it is unclear what the eastern basin geometry was like before the onset of Neogene distortion.

[42] We speculate that the initiation of subduction in this location at 25–22 Ma was near the thinnest part of the crust, based upon the correlation between the thickness of the upper plate and the location of the plate edge near East Cape Ridge (Figures 3 and 9).

[43] Below the fore-arc crust, we measured an upper mantle Vp of 8.05 ± 0.15 km which is typical for normal, unaltered mantle without serperntinization induced by hydration [*Carlson and Miller*, 2003]. *Bostock et al.* [2002] speculate that all mantle wedges would be serpentinized, and this would inhibit subduction zone thrust earthquakes to rupture below the Moho interception [*Tichelaar and Ruff*, 1993]. Our measurements, however, imply a nonserpentinized mantle wedge at the Moho interception, and so the northern Hikurangi margin may have a different megathrust earthquake potential than otherwise assumed.

6.3. East Cape Ridge Volcanics

[44] We detected relatively high seismic velocities (about 5.8 km/s) at 3.5 km depth below the seafloor at East Cape Ridge (Figure 3). We also model a source region for the observed magnetic anomaly that approximately coincides with this seismic anomaly (Figures 7 and 8). We interpret the high-velocity magnetic material to be volcanic and consider possibilities that the source material is: a seamount that was subducted and accreted; or part of allochthonous unit Y within the basin [*Sutherland et al.*, 2009] and a correlative to the Matakaoa Volcanic unit mapped onshore [*Mazengarb and Speden*, 2000]; or that it represents basement to Raukumara Basin that has been uplifted.

[45] Fore-arc accretion of seamounts from the Hikurangi Plateau may be likely in this region [*Davey et al.*, 1997; *Henrys et al.*, 2006; *Pecher et al.*, 2005] because the subducting Hikurangi Plateau has numerous seamounts visible in the bathymetry (Figure 1) [*Wood and Davy*, 1994]. It has been speculated that in the vicinity of our study area subducted seamounts are required to explain localized uplift, erosion and basin evolution [*Collot et al.*, 2001; *Lewis et al.*, 2004]. Consideration of the model location and dimension

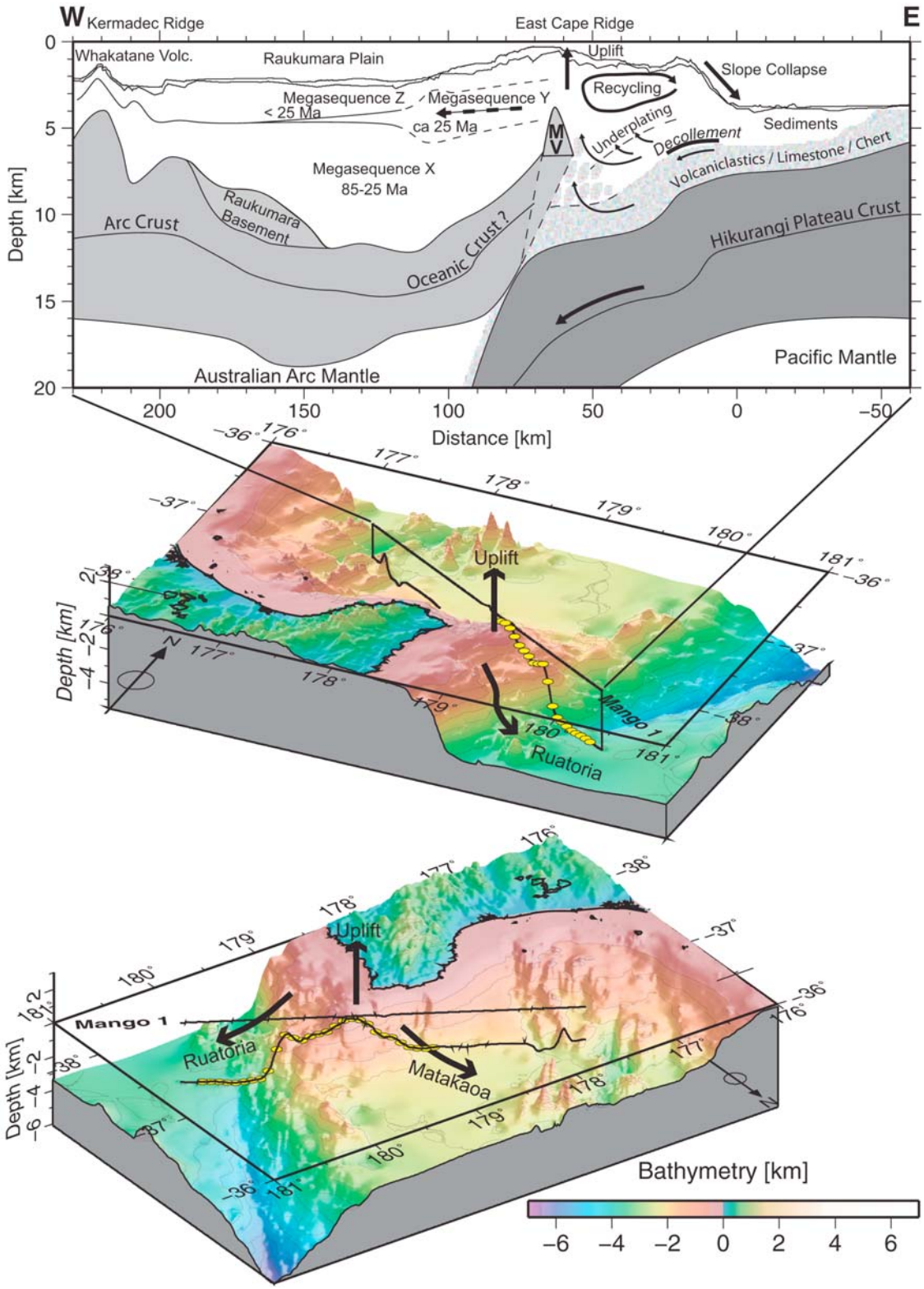

Figure 9. (top) Summary of structural interpretation, with concepts of material recycling within the subduction wedge (right in Figure 9 (top)) and uplift and mass wasting focused at the shallow East Cape Ridge near our data profile (see also (middle and bottom) three-dimensional views). Here, we also detected a strong shallow high velocity and strong magnetic anomalous rock (marked as "MV" in Figure 9 (top)) which is also interpreted as the source region for megasequence Y, indicated by dashed arrow (center in Figure 9 (top)).

of the specific anomaly, which lies 10 km above the subduction interface at East Cape Ridge, requires a detached and uplifted seamount. If a seamount of 1–2 km elevation, which is the average for the Hikurangi Plateau, was subducted and detached from the downgoing plate, then it has experienced an uplift of 8–9 km from the subduction interface and has attained that height against its negative buoyancy. The large rock uplift value suggests that it was accreted from the downgoing plate and has since undergone a long history of further subduction and basal accretion. Although this scenario would explain the lack of any detectable scar at the trench, we consider it unlikely that such a scenario is mechanically feasible. However, we have not made any mechanical model to simulate this process and retain it as a hypothesis.

[46] There are several magnetic anomalies associated with East Cape Ridge that have similar amplitude and wavelength and are aligned parallel to the ridge (Figure 6). The most southwestern anomaly corresponds to where the Matakaoa Volcanics unit is mapped onshore as part of an allochthonous unit emplaced at 25–22 Ma [*Mazengarb and Speden*, 2000]. Based upon our Euler deconvolution analysis (Figure 8), we note a correlation between seismic reflection megasequence Y (Figure 9), which is a correlative of the onshore allochthon [*Sutherland et al.*, 2009], and model sources of magnetization (Figure 8). As this unit is supposed to represent a slump from the southeast, now the region of East Cape Ridge, the magnetization indicates that the highly magnetic high velocity anomaly below East Cape Ridge could either be a correlative of the unit, or could be the slump source (large dashed arrow in Figure 9). Therefore, we conclude that we have very likely detected an offshore part of the Matakaoa volcanics within allochthonous megasequence Y, and our results support the conclusion by *Davey et al.* [1997] that the onshore allochthon volcanic geology extends further northeast along East Cape Ridge.

[47] The seismic velocity of the anomaly beneath East Cape Ridge (approximately 5.8 km/s) is relatively similar to that of the adjacent upper Australian crust beneath Raukumara Basin (5.4–5.8 km/s) and faster than that of the upper Hikurangi Plateau crust (4.9 km/s). Thus, the origin of the seismic and magnetic anomaly beneath East Cape Ridge could be from uplifted basement of Raukumara Basin, which in turn may be the source of allochthonous material that was emplaced into the basin during subduction initiation as the Matakaoa Volcanics and seismic reflection megasequence Y. *Cassidy* [1993] reports magnetizations of up to 5.5 A/m from similar allochthonous units in Northland that were also emplaced at 25–22 Ma, so our estimate of 3.3–3.9 A/m seems reasonable and may imply a common origin of the material.

6.4. Tectonic Erosion and Accretion Between East Cape Ridge and the Trench

[48] We interpret the frontal 100 km of the fore arc, from East Cape Ridge to the Hikurangi Trench, to be highly dynamic and actively deforming. Our structural model (Figures 3 and 5) exhibits relatively slow seismic velocities and high seismic attenuation in this region. It is bound to the east by the high-velocity anomaly that lies beneath East Cape Ridge. Figure 9 shows our structural interpretation. In the following, we use structural and geometrical arguments to characterize the fore-arc deformation mechanism in this region.

[49] The slope of the seafloor near the deformation front is relatively steep (~11° over a distance of 13 km in water depths of 3600 to 1100 m). High-resolution bathymetry and seismic data reveal a highly-faulted slope of acoustically reflective indurated material, apparently indicative of collapse and subduction erosion [*Collot and Davy*, 1998]. Oversteepening of trench slopes by subduction erosion can lead to dramatic, possibly tsunamogenic avalanches [*von Huene et al.*, 1989].

[50] Margin slopes can be used to distinguish between erosive and accretive margin types; however, wavelengths above 50 km need to be examined [*Clift and Vannucchi*, 2004]. The frontal fore-arc slope of our profile is around 3° over the distance from East Cape Ridge to the trench. This is steeper than observed globally at accretive margins and could, therefore, be considered as evidence for an erosive subduction margin [*Clift and Vannucchi*, 2004]. However, allowing for the shallow subduction angle of the plateau crust (~4° within 70 km of the deformation front), the taper angle is relatively shallow (7°). In global comparison, this low taper angle is not clearly erosive [*Clift and Vannucchi*, 2004], and taking into account the trench sediment supply of about 2 km and the orthogonal plate convergence rate of 60 km/Myr, the northern Hikurangi margin exhibits characteristics more consistent with an accretive margin setting [*Clift and Vannucchi*, 2004].

[51] Another argument against net subduction erosion at the margin is given by *Sutherland et al.* [2009]. They argue that tectonic erosion of the fore arc would lead to trench retreat over geologic time. Hence the Hikurangi volcanic arc would have moved westward with time, relative to Raukumara Basin, to preserve the distance between the deformation front and the arc volcanoes [*Lallemand*, 1995]. However, *Sutherland et al.* [2009] present evidence that extinct arc volcanoes are not present within the basin and hence suggest little or no net tectonic erosion of the fore arc since 22 Ma.

[52] An alternative mechanism to consider is that of lower-crustal underplating and hence fore-arc uplift caused by continuity of volume, i.e., without an increase in the total volume of the fore arc. Rather than being accreted at the toe of the fore-arc wedge, incoming sedimentary material enters a subduction channel and then, because it is too buoyant and weak to penetrate beneath the overriding mantle wedge, it is transferred upward across the subduction thrust and is underplated to the fore-arc crust to form the root of the outer fore-arc high. This mechanism was first suggested for Raukumara Peninsula by *Walcott* [1987], and was developed by *Sutherland et al.* [2009] to include both subducted sediment and material derived from frontal subduction erosion to explain the geometry and uplift of East Cape Ridge.

[53] With our new geometrical constraints we are able to test and quantify the fore-arc kinematic model of *Sutherland et al.* [2009]. The region between the trench and East Cape Ridge consists of material of relatively low seismic velocities (3.3 km/s at 6 km below the seafloor) and low sedimentary densities (<2.3 g/cm^3), as indicated by the depression of the sedimentary bodies at model km 40 in Figures 3 and 7. In

addition, we infer high seismic attenuation east of model km 100 based upon weak refracted signals and the incoherent seismic reflection character of MCS data (Figures 2b–2e and 5), as corroborated by seismological results for the Raukumara region to the south [*Eberhart-Phillips and Chadwick*, 2002]. We attribute these seismic and density characteristics to the considerable internal deformation of the accreted and recycled fore arc. Similar observations were made at the fore-arc high of the Sunda-Banda arc transition [*Shulgin et al.*, 2009], where the source of the material is attributed to basal accretion based on numerical modeling [*Selzer et al.*, 2008].

[54] Our identification of the material that is being recycled or actively accreted to the fore arc allows us to perform simplified calculations of mass fluxes at the subduction zone since the Neogene at 22 Ma, by taking into account the plate convergence, back-arc opening, and assuming an average thickness for the incoming sediments. The total convergence at the subduction zone at this location since 22 Ma is assumed to be the sum of the plate motion of 880 km, as computed from the rotations of *Cande and Stock* [2004], and the back-arc opening in the Havre Trough of approximately 120 km. The input of the subduction zone that is available for accretion is the sediment thickness on the downgoing plate, and any volcanics (e.g., seamounts) that could detach, integrated over the 22 Myr history of convergence. We identify 4 km of material currently entering the subduction system on our cross section: 2.2 km of sediments inferred to have collapsed off the adjacent trench slope, plus almost 2 km of some basal volcaniclastics which may be classified as part of the oceanic crust. The proximity of our profile to the Ruatoria Debris Avalanche [*Collot et al.*, 2001] results in an overestimation of how much material is added on average from outside the system; about 1 km less trench fill is observed today on seismic lines north and south of the Ruatoria Debris Avalanche. In general, the sediment thickness found on the Hikurangi Plateau away from the active trench is <1 km [*Davy et al.*, 2008], and so we estimate the total input to be 1000 ± 500 km^2. The total volume of accreted and recycled fore-arc material beneath the trench slope is estimated from our cross section to be 500 ± 50 km^2, so our best estimate is that half of the incoming material has been accreted to the margin, though the possible range is 25–100%. Crustal material may leave the fore arc through erosion into sedimentary basins to the east or west, or may be subducted into the mantle. The volumes of Neogene basins surrounding East Cape Ridge are large, but the sedimentary fill is mostly composed of clasts transported from onshore New Zealand and minor volcaniclastic input. Therefore, we cannot determine the proportion that is eroded from East Cape Ridge, but we can identify a large enough reservoir to potentially account for all of the remaining deficit in mass flux.

[55] A similar suggestion of close to zero net balance of subduction zone material transfer is made for the eastern Sunda Arc region (E. Lueschen et al., Structure, evolution and tectonic activity of the eastern Sunda forearc, Indonesia, from marine seismic investigations, submitted to Tectonophysics, 2009) that may extend as far as east of Sumba Island in the east [*Shulgin et al.*, 2009; *Planert et al.*, 2010] and Java Island in the west [*Kopp et al.*, 2006]. Another recycling system is described for the paleoaccretionary wedge in south-central Chile [*Glodny et al.*, 2005] though only an uplift and erosion balance is estimated without considering the total mass budget. And another area of pronounced uplift of the outer fore-arc high but subsidence and collapse of the trench slope is reported at the Tonga trench [*Clift et al.*, 1998], where we propose that underplating of the fore-arc crust may have been partly overlooked due to a lack of data. The steep slopes in these regions indicate a relatively high basal friction and may have higher input than output to form a pronounced outer fore-arc high [*Gutscher et al.*, 1998].

[56] Of particular interest for global models of crustal growth is the flux of material with a continental chemistry that is transported back into the mantle at subduction zones, because it is widely believed that this must be in approximate balance with the rate of production of new continental crust at volcanic arcs [e.g., *von Huene and Scholl*, 1991; *Clift and Vannucchi*, 2004; *Hawkesworth and Kemp*, 2006]. It has been widely assumed that margins with evidence for subsidence and collapse of the trench slope are regions of trench retreat and long-term recycling of fore-arc crust into the mantle [e.g., *Clift and Vannucchi*, 2004], but we challenge the underlying assumption used to estimate these rates. According to the model suggested by *Sutherland et al.* [2009] and our determination of the volume of accreted material at East Cape Ridge, past estimates of the rate of crustal recycling into the mantle could be greater than the true value because the significance of underplating at the base of the crust may not have been fully recognized. Our observations may go a long way towards explaining the discrepancy between independent estimates of crustal growth at arcs [*Reymer and Schubert*, 1984] and crustal destruction at subduction zones [*Clift and Vannucchi*, 2004].

7. Conclusions

[57] Seismic wide-angle and vertical reflection data together with gravity and magnetic anomalies have been used to determine lithospheric structures of the northern Hikurangi margin, where the Hikurangi Plateau subducts beneath the Raukumara fore-arc basin. A combination of seismic ray-tracing modeling, seismic stratigraphy, gravity and magnetic modeling reveal the structure and deformation of the subduction zone as well as the origin and possible age of certain rock units.

[58] The shallow structure of the Hikurangi Plateau as determined by seismic wide-angle data consists at the Hikurangi trench of up to 2 km sediments with seismic velocities up to 3.5 km/s above a unit of about 2 km of seismically faster (>3.8 km/s) volcaniclastic, limestone, and chert material. The underlying crust is composed of an upper, 4 km thick layer with velocities of 4.9–6.7 km/s above the lower crust which is characterized by velocities >7.1 km/s. The Moho depth was estimated by gravity modeling and could not be verified by the seismic data. The thickness of the plateau is approximately 10 km.

[59] The Raukumara fore-arc basin represents one of the deepest known (>10 km thick) fore-arc basins, and formed initially during the Mesozoic Gondwana subduction episode, but was reactivated during the Neogene Hikurangi subduction [*Sutherland et al.*, 2009]. This reactivation process may be the only mechanism that creates such superdeep

fore-arc basins. Raukumara Basin developed on a 5–10 km thick crust. Up to 6 km of Cretaceous and Paleogene sediment was deposited over the thinnest part of the crust, which was then overlain by an allochthon that was emplaced at 25–22 Ma. We infer sourced Matakaoa volcanic material from uplifted basement exposed on a precursor to East Cape Ridge, where a high velocity, highly magnetized anomaly point to Matakaoa volcanics exposed onshore. Neogene sediments up to 3 km thick were then deposited on top of this allochthon [*Sutherland et al.*, 2009]. Refractions from the fore-arc mantle indicate seismic velocities above 8 km/s, implying that outside the region of arc volcanism the mantle material appears unaltered. Below Raukumara Basin, seismic reflections off the subducting slab indicate that the inclination of the initially low-angled slab dip steepens to over 10°, and, according to seismicity, steepens further to almost 50° below the arc.

[60] The East Cape Ridge to the trench is a 100 km wide region that is experiencing uplift due to underplating of relatively low-seismic-velocity and low-density crust from a subduction channel. The limited depth penetration of seismic data indicates high seismic attenuation attributed to significant internal deformation related to material recycling within the hanging wall wedge. Uplift of the fore arc causes oversteepening of the frontal taper, and material collapses and enters into the subduction channel from which it can become underplated and uplifted again.

[61] A mass balance calculation indicates that the low-seismic-velocity, high-attenuation, low-density fore-arc crust that we image beneath the trench slope and interpret to be accreted and recycled material represents 25–100% of the incoming sediment from the downgoing plate, and that the remainder could be accounted for through erosion of older accreted material into surrounding sedimentary basins. We suggest that previous estimates of continental mass flux into the mantle at subduction zones may be overestimated because they have not properly accounted for crustal underplating beneath fore-arc highs.

[62] **Acknowledgments.** We thank Captain Mallon and the crew of R/V *Sonne* for a smooth and efficient acquisition of the seismic wide-angle data, the New Zealand National Institute of Water and Atmospheric Research (NIWA) for providing high-resolution bathymetry of the research area, the Editor and two anonymous reviewers for their helpful and highly constructive reviews, and finally the German Ministry for Education and Research (BMBF), the German Research foundation (DFG), the New Zealand Foundation for Research Science and Technology (FRST), the New Zealand Ministry for Economic Development (MED) for funding various aspects of this research. Most figures were made with GMT [*Wessel and Smith*, 1998].

References

Árnadóttir, T., S. Thornley, F. F. Pollitz, and D. J. Darby (1999), Spatial and temporal strain rate variations at the northern Hikurangi margin, New Zealand, *J. Geophys. Res.*, *104*(B3), 4931–4944, doi:10.1029/1998JB900109.

Barker, D. H. N., R. Sutherland, S. Henrys, and S. Bannister (2009), Geometry of the Hikurangi subduction thrust and upper plate, North Island, New Zealand, *Geochem. Geophys. Geosyst.*, *10*, Q02007, doi:10.1029/2008GC002153.

Bialas, J., and E. R. Flueh (1999), Ocean bottom seismometers, *Sea Technol.*, *40*(4), 41–46.

Bostock, M. G., R. D. Hyndman, S. Rondenay, and S. M. Peacock (2002), An inverted continental Moho and serpentinization of the forearc mantle, *Nature*, *417*, 536–538, doi:10.1038/417536a.

Cande, S. C., and J. M. Stock (2004), Pacific-Antarctic-Australia motion and the formation of the Macquarie Plate, *Geophys. J. Int.*, *157*, 399–414, doi:10.1111/j.1365-246X.2004.02224.x.

Carlson, R. L., and D. J. Miller (2003), Mantle wedge water contents estimated from seismic velocities in partially serpentinized peridotites, *Geophys. Res. Lett.*, *30*(5), 1250, doi:10.1029/2002GL016600.

Cassidy, J. (1993), Tectonic implications of paleomagnetic data from the Northland Ophiolite, *New Zealand, Tectonophysics*, *223*(3–4), 199–211, doi:10.1016/0040-1951(93)90138-A.

Clift, P. D., and P. Vannucchi (2004), Controls on tectonic accretion versus erosion in subduction zones: Implications for the origin and recycling of the continental crust, *Rev. Geophys.*, *42*, RG2001, doi:10.1029/2003RG000127.

Clift, P. D., C. J. MacLeod, D. R. Tappin, D. J. Wright, and S. H. Bloomer (1998), Tectonic controls on sedimentation and diagenesis in the Tonga Trench and forearc, southwest Pacific, *Geol. Soc. Am. Bull.*, *110*(4), 483–496, doi:10.1130/0016-7606(1998)110<0483:TCOSAD>2.3.CO;2.

Cloos, M. (1993), Lithospheric buoyancy and collisional orogenesis: subduction of oceanic plateaus, continental margins, island arcs, spreading ridges, and seamounts, *Geol. Soc. Am. Bull.*, *105*, 715–737, doi:10.1130/0016-7606(1993)105<0715:LBACOS>2.3.CO;2.

Coffin, M. F., and O. Eldholm (1994), Large igneous provinces: Crustal structure, dimensions, and external consequences, *Rev. Geophys.*, *32*(1), 1–36, doi:10.1029/93RG02508.

Collot, J.-Y., and B. Davy (1998), Forearc structures and tectonic regimes at the oblique subduction zone between the Hikurangi Plateau and the southern Kermadec margin, *J. Geophys. Res.*, *103*(B1), 623–650, doi:10.1029/97JB02474.

Collot, J.-Y., et al. (1996), From subduction to intra-continental transpression: Structures of the southern Kermadec-Hikurangi margin from multibeam bathymetry, side-scan sonar, and seismic reflection, *Mar. Geophys. Res.*, *18*, 357–381, doi:10.1007/BF00286085.

Collot, J.-Y., K. B. Lewis, G. Lamarche, and S. Lallemand (2001), The giant Ruatoria debris avalanche on the northern Hikurangi margin, New Zealand: Result of oblique seamount subduction, *J. Geophys. Res.*, *106*(B9), 19,271–19,297, doi:10.1029/2001JB900004.

Cooper, G. R. J. (2002), An improved algorithm for the Euler deconvolution of potential field data, *Leading Edge*, *21*(12), 1197–1198, doi:10.1190/1.1536132.

Cooper, G. R. J. (2004), A semi-automatic procedure for the interpretation of geophysical data, *Explor. Geophys.*, *35*, 182–187, doi:10.1071/EG04182.

Davey, F. J., M. Hampton, J. Childs, M. A. Fisher, K. Lewis, and J. R. Pettinga (1986), Structure of a growing accretionary prism, Hikurangi margin, New Zealand, *Geology*, *14*, 663–666, doi:10.1130/0091-7613(1986)14<663:SOAGAP>2.0.CO;2.

Davey, F. J., S. Henrys, and E. Lodolo (1997), A seismic crustal section across the East Cape convergent margin, New Zealand, *Tectonophysics*, *269*, 199–215, doi:10.1016/S0040-1951(96)00165-5.

Davis, D. M., J. Suppe, and F. A. Dahlen (1983), Mechanics of fold-and-thrust belts and accretionary wedges, *J. Geophys. Res.*, *88*, 1153–1172, doi:10.1029/JB088iB02p01153.

Davy, B., and J.-Y. Collot (2000), The Rapuhia Scarp (northern Hikurangi Plateau): Its nature and subduction effects on the Kermadec Trench, *Tectonophysics*, *328*, 269–295, doi:10.1016/S0040-1951(00)00211-0.

Davy, B., and R. Wood (1994), Gravity and magnetic modeling of the Hikurangi Plateau, *Mar. Geol.*, *118*(1–2), 139–151, doi:10.1016/0025-3227(94)90117-1.

Davy, B., K. Hoernle, and R. Werner (2008), Hikurangi Plateau: Crustal structure, rifted formation, and Gondwana subduction history, *Geochem. Geophys. Geosyst.*, *9*, Q07004, doi:10.1029/2007GC001855.

de Ronde, C., et al. (2007), Submarine hydrothermal activity along the mid-Kermadec Arc, New Zealand: Large scale effects on venting, *Geochem. Geophys. Geosyst.*, *8*, Q07007, doi:10.1029/2006GC001495.

DeMets, C., R. G. Gordon, D. F. Argus, and S. Stein (1994), Effect of recent revisions to the geomagnetic time scale on estimates of current plate motions, *Geophys. Res. Lett.*, *21*, 2191–2194, doi:10.1029/94GL02118.

Durrheim, R. J., and G. R. J. Cooper (1998), Euldep: A program for the Euler deconvolution of magnetic and gravity data, *Comput. Geosci.*, *24*, 545–550, doi:10.1016/S0098-3004(98)00022-3.

Eberhart-Phillips, D., and M. Chadwick (2002), Three-dimensional attenuation model of the shallow Hikurangi subduction zone in the Raukumara Peninsula, New Zealand, *J. Geophys. Res.*, *107*(B2), 2033, doi:10.1029/2000JB000046.

Field, B. D., et al. (1997), *Cretaceous-Cenozoic Geology and Petroleum Systems of the East Coast Region, New Zealand*, *Geol. Monogr. Ser.*, vol. 19, 301 pp., GNS Sci., Lower Hutt, New Zealand.

Flueh, E. R., and H. Kopp (2007), FS Sonne Fahrtbericht/cruise report SO192 MANGO: Marine geoscientific investigations on the input and output of the Kermadec subduction zone, Rep. 11, 127 pp., IFM-GEOMAR, Kiel, Germany.

Gillies, P. N. (1984), A marine geophysical study of the junction of the Kermadec and Hikurangi subduction systems, Ph.D. thesis, Univ. of Auckland, Aukland, New Zealand.

Glodny, J., J. Lohrmann, H. Echtler, K. Gräfe, W. Seifert, S. Collao, and O. Figueroa (2005), Internal dynamics of a paleoaccretionary wedge: Insights from combined isotope tectonochronology and sandbox modelling of the South-Central Chilean forearc, *Earth Planet. Sci. Lett.*, *231* (1–2), 23–39, doi:10.1016/j.epsl.2004.12.014.

Gutscher, M.-A., N. Kukowski, J. Malavieille, and S. Lallemand (1998), Material transfer in accretionary wedges from analysis of a systematic series of analog experiments, *J. Struct. Geol.*, *20*(4), 407–416, doi:10.1016/S0191-8141(97)00096-5.

Hawkesworth, C. J., and A. I. S. Kemp (2006), Evolution of the continental crust, *Nature*, *443*, 811–817, doi:10.1038/nature05191.

Henrys, S. A., M. Reyners, I. Pecher, S. Bannister, Y. Nishimura, and G. Maslen (2006), Kinking of the subducting slab by escalator normal faulting beneath the North Island of New Zealand, *Geology*, *34*(9), 777–780, doi:10.1130/G22594.22591.

Herzer, R. H. (1995), Seismic stratigraphy of a buried volcanic arc, Northland, New Zealand and implications for Neogene subduction, *Mar. Pet. Geol.*, *12*(5), 511–531, doi:10.1016/0264-8172(95)91506-K.

Hoernle, K., F. Hauff, R. Werner, and N. Mortimer (2004), New insights into the origin and evolution of the Hikurangi oceanic plateau, *Eos Trans. AGU*, *85*(41), 401–416, doi:10.1029/2004EO410001.

Kopp, H., and N. Kukowski (2003), Backstop geometry and accretionary mechanics of the Sunda margin, *Tectonics*, *22*(6), 1072, doi:10.1029/2002TC001420.

Kopp, H., et al. (2006), The Java margin revisited: Evidence for subduction erosion off Java, *Earth Planet. Sci. Lett.*, *242*(1–2), 130–142, doi:10.1016/j.epsl.2005.11.036.

Lallemand, S. (1995), High-rates of arc consumption by subduction processes: Some consequences, *Geology*, *23*(6), 551–554, doi:10.1130/0091-7613(1995)023<0551:HROACB>2.3.CO;2.

Lamarche, G., C. Joanne, and J.-Y. Collot (2008), Successive, large mass-transport deposits in the south Kermadec fore-arc basin, New Zealand: The Matakaoa Submarine Instability Complex, *Geochem. Geophys. Geosyst.*, *9*, Q04001, doi:10.1029/2007GC001843.

Lewis, K. B., J.-Y. Collot, and S. E. Lallemand (1998), The dammed Hikurangi Trough: A channel-fed trench blocked by subducting seamounts and their wake avalanches (New Zealand-France GeodyNZ Project), *Basin Res.*, *10*, 441–468, doi:10.1046/j.1365-2117.1998.00080.x.

Lewis, K. B., S. Lallemand, and L. Carter (2004), Collapse in a Quaternary shelf basin off East Cape, New Zealand: Evidence for passage of a subducted seamount inboard of the Ruatoria giant avalanche, *N. Z. J. Geol. Geophys.*, *47*(3), 415–429.

Litchfield, N., S. Ellis, K. Berryman, and A. Nicol (2007), Insights into subduction-related uplift along the Hikurangi margin, New Zealand, using numerical modeling, *J. Geophys. Res.*, *112*, F02021, doi:10.1029/2006JF000535.

Malahoff, A., R. H. Feden, and H. S. Fleming (1982), Magnetic anomalies and tectonic fabric of marginal basins north of New Zealand, *J. Geophys. Res.*, *87*(B5), 4109–4125, doi:10.1029/JB087iB05p04109.

Mann, P., and A. Taira (2004), Global tectonic significance of the Solomon Islands and Ontong Java Plateau convergent zone, *Tectonphysics*, *389*(3–4), 137–190, doi:10.1016/j.tecto.2003.10.024.

Mazengarb, C., and D. H. M. Harris (1994), Cretaceous stratigraphic and structural relationships of Raukumara Peninsula, New Zealand; stratigraphic patterns associated with the migration of a thrust system, *Ann. Tecton.*, *8*(2), 100–118.

Mazengarb, C., and I. G. Speden (2000), Geology of the Raukumara area, geological map, 60 pp., scale 1:250,000, GNS Sci., Lower Hutt, New Zealand.

McGeary, S., A. Nur, and Z. Ben-Avraham (1985), Spatial gaps in arc volcanism: The effect of collision or subduction of oceanic plateaus, *Tectonophysics*, *119*, 195–221, doi:10.1016/0040-1951(85)90039-3.

McIntosh, K. D., E. A. Silver, I. Ahmed, A. Berhorst, C. R. Ranero, R. K. Kelly, and E. R. Flueh (2007), The Nicaragua convergent margin: Seismic reflection imaging of the source of a tsunami earthquake, in *The Seismogenic Zone of Subduction Subduction Thrust Faults*, edited by T. Dixon and J. C. Moore, pp. 257–287, Columbia Univ. Press, New York.

Mortimer, N., and D. Parkinson (1996), Hikurangi Plateau: A Cretaceous large igneous province in the southwest Pacific Ocean, *J. Geophys. Res.*, *101*, 687–696, doi:10.1029/95JB03037.

Nicol, A., C. Mazengarb, F. Chanier, G. Rait, C. Uruski, and L. Wallace (2007), Tectonic evolution of the active Hikurangi subduction margin, New Zealand, since the Oligocene, *Tectonics*, *26*, TC4002, doi:10.1029/2006TC002090.

Park, J.-O., T. Tsuru, S. Kodaira, P. R. Cummins, and Y. Kaneda (2002), Splay fault branching along the Nankai subduction zone, *Science*, *297*, 1157–1160, doi:10.1126/science.1074111.

Pecher, I. A., S. A. Henrys, S. Ellis, S. M. Chiswell, and N. Kukowski (2005), Erosion of the seafloor at the top of the gas hydrate stability zone on the Hikurangi margin, New Zealand, *Geophys. Res. Lett.*, *32*, L24603, doi:10.1029/2005GL024687.

Planert, L., H. Kopp, E. Lueschen, C. Mueller, E. R. Flueh, A. Shulgin, Y. Djajadihardja, and A. Krabbenhoeft (2010), Lower plate structure and upper plate deformational segmentation at the Sunda-Banda arc transition, Indonesia, *J. Geophys. Res.*, doi:10.1029/2009JB006713, in press.

Rait, G., F. Chanier, and D. W. Waters (1991), Landward- and seaward-directed thrusting accompanying the onset of subduction beneath New Zealand, *Geology*, *19*(3), 230–233, doi:10.1130/0091-7613(1991)019<0230:LASDTA>2.3.CO;2.

Ranero, C. R., R. von Huene, E. R. Flueh, M. Duarte, D. Baca, and K. McIntosh (2000), A cross section of the convergent Pacific margin of Nicaragua, *Tectonics*, *19*(2), 335–357.

Reymer, A., and G. Schubert (1984), Phanerozoic addition rates to the continental crust and crustal growth, *Tectonics*, *3*(1), 63–77, doi:10.1029/TC003i001p00063.

Reyners, M., and P. McGinty (1999), Shallow subduction tectonics in the Raukumara Peninsula, New Zealand, as illuminated by earthquake focal mechanisms, *J. Geophys. Res.*, *104*, 3025–3034, doi:10.1029/1998JB900081.

Reyners, M., D. Eberhart-Phillips, and G. Stuart (1999), A three-dimensional image of shallow subduction: crustal structure of the Raukumara Peninsula, New Zealand, *Geophys. J. Int.*, *137*(3), 873–890, doi:10.1046/j.1365-246x.1999.00842.x.

Reyners, M., D. Eberhart-Phillips, G. Stuart, and Y. Nishimura (2006), Imaging subduction from the trench to 300 km depth beneath the central North Island, New Zealand, with Vp and Vp/Vs, *Geophys. J. Int.*, *165*, 565–583, doi:10.1111/j.1365-246X.2006.02897.x.

Rudnick, R. L., and D. M. Fountain (1995), Nature and composition of the continental crust: A lower crustal perspective, *Rev. Geophys.*, *33*(3), 267–309, doi:10.1029/95RG01302.

Sandwell, D. T., and W. H. F. Smith (1997), Marine gravity from Geosat and ERS-1 altimetry, *J. Geophys. Res.*, *102*, 10,039–10,054, doi:10.1029/96JB03223.

Selzer, C., S. J. H. Buiter, and O. A. Pfiffner (2008), Numerical modeling of frontal and basal accretion at collisional margins, *Tectonics*, *27*, TC3001, doi:10.1029/2007TC002169.

Shulgin, A., H. Kopp, C. Mueller, E. Lueschen, L. Planert, M. Engels, E. R. Flueh, A. Krabbenhoeft, and Y. Djajadihardja (2009), Sunda-Banda arc transition: Incipient continent-island arc collision (northwest Australia), *Geophys. Res. Lett.*, *36*, L10304, doi:10.1029/2009GL037533.

Song, T. R. A., and M. Simons (2003), Large trenchparallel gravity variations predict seismogenic behavior in subduction zones, *Science*, *301*, 630–633, doi:10.1126/science.1085557.

Sutherland, R., et al. (2009), Reactivation of tectonics, crustal underplating, and uplift after 60 Myr of passive subsidence, Raukumara Basin, Hikurangi-Kermadec fore arc, New Zealand: Implications for global growth and recycling of continents, *Tectonics*, *28*, TC5017, doi:10.1029/2008TC002356.

Thornley, S. (1996), Neogene tectonics of Raukumara Peninsula, northern Hikurangi margin, New Zealand, Ph.D. thesis, Victoria Univ. of Wellington, Wellington.

Tichelaar, B. W., and L. J. Ruff (1993), Depth of seismic coupling along subduction zones, *J. Geophys. Res.*, *98*(B2), 2017–2037, doi:10.1029/92JB02045.

Upton, P., P. O. Koons, and D. Eberhart-Phillips (2003), Extension and partitioning in an oblique subduction zone, New Zealand: Constraints from three-dimensional numerical modeling, *Tectonics*, *22*(6), 1068, doi:10.1029/2002TC001431.

von Huene, R., and D. W. Scholl (1991), Observations at convergent margins concerning sediment subduction, subduction erosion, and the growth of continental crust, *Rev. Geophys.*, *29*, 279–316, doi:10.1029/91RG00969.

von Huene, R., J. Bourgois, J. Miller, and G. Pautot (1989), A large tsunamogenic landslide and debris flow along the Peru trench, *J. Geophys. Res.*, *94*(B2), 1703–1714, doi:10.1029/JB094iB02p01703.

von Huene, R., C. R. Ranero, and P. Vannucchi (2004), Generic model of subduction erosion, *Geology*, *32*(10), 913–916, doi:10.1130/G20563.1.

Walcott, R. I. (1987), Geodetic strain and the deformational history of the North Island of New Zealand during the late Cainozoic, *Philos. Trans. R. Soc. London A*, *321*, 163–181, doi:10.1098/rsta.1987.0009.

Wallace, L. M., J. Beavan, R. McCaffrey, and D. Darby (2004), Subduction zone coupling and tectonic block rotations in the North Island, New Zealand, *J. Geophys. Res.*, *109*, B12406, doi:10.1029/2004JB003241.

Wallace, L. M., et al. (2009), Characterizing the seismogenic zone of a major plate boundary subduction thrust: Hikurangi margin, New Zealand, Geochem. *Geochem. Geophys. Geosyst.*, *10*, Q10006, doi:10.1029/2009GC002610.

Walther, C. H. E., E. R. Flueh, C. R. Ranero, R. von Huene, and W. Strauch (2000), Crustal structure across the Pacific margin of Nicaragua: Evidence for ophiolitic basement and a shallow mantle sliver, *Geophys. J. Int.*, *141*, 759–777, doi:10.1046/j.1365-246x.2000.00134.x.

Wells, R. E., R. J. Blakely, Y. Sugiyama, D. W. Scholl, and P. A. Dinterman (2003), Basin-centered asperities in great subduction zone earthquakes: A link between slip, subsidence, and subduction erosion?, *J. Geophys. Res.*, *108*(B10), 2507, doi:10.1029/2002JB002072.

Wessel, P., and W. H. S. Smith (1998), New version of generic mapping tools released, *Eos Trans. AGU*, *79*, 579, doi:10.1029/98EO00426.

Whattam, S. A., J. G. Malpas, J. R. Ali, I. E. M. Smith, and C. H. Lo (2004), Origin of the Northland Ophiolite, northern New Zealand: Discussion of new data and reassessment of the model, *N. Z. J. Geol. Geophys.*, *47*(3), 383–389.

Wilson, K., K. Berryman, U. Cochran, and T. Little (2007), Holocene coastal evolution and uplift mechanisms of the northeastern Raukumara Peninsula, North Island, New Zealand, *Quat. Sci. Rev.*, *26*(7–8), 1106–1128, doi:10.1016/j.quascirev.2007.01.005.

Wood, R., and B. Davy (1994), The Hikurangi Plateau, *Mar. Geol.*, *118*(1–2), 153–173, doi:10.1016/0025-3227(94)90118-X.

Ye, S., E. R. Flueh, D. Klaeschen, and R. von Huene (1997), Crustal structure along the EDGE transect beneath the Kodiak shelf off Alaska derived from OBH seismic refraction data, *Geophys. J. Int.*, *130*(2), 283–302, doi:10.1111/j.1365-246X.1997.tb05648.x.

Zelt, C. A. (1999), Modelling strategies and model assessment for wide-angle seismic traveltime data, *Geophys. J. Int.*, *139*, 183–204, doi:10.1046/j.1365-246X.1999.00934.x.

Zelt, C. A., and R. B. Smith (1992), Seismic traveltime inversion for 2-D crustal velocity structure, *Geophys. J. Int.*, *108*, 16–34, doi:10.1111/j.1365-246X.1992.tb00836.x.

D. H. N. Barker, S. A. Henrys, M. E. Reyners, V. M. Stagpoole, and R. Sutherland, GNS Science, P.O. Box 30-368, Lower Hutt 5040, New Zealand.

D. G. Bassett, School of Geography, Environment and Earth Sciences, Victoria University of Wellington, P.O. Box 600, Wellington 6140, New Zealand.

A. Dannowski, E. R. Flueh, H. Kopp, and L. Planert, Leibniz Institute of Marine Sciences, IFM-GEOMAR, Wischhofstr. 1-3, D-24148 Kiel, Germany.

M. Scherwath, School of Earth and Ocean Sciences, University of Victoria, P.O. Box 3065, STN CSC, Victoria, BC V8W 3V6, Canada. (mscherwa@uvic.ca)